Protein Delivery

DOI: 10.1002/anie.201410006

Covalent Attachment of Cyclic TAT Peptides to GFP Results in Protein Delivery into Live Cells with Immediate Bioavailability**

Nicole Nischan, Henry D. Herce, Francesco Natale, Nina Bohlke, Nediljko Budisa, M. Cristina Cardoso, and Christian P. R. Hackenberger**

Abstract: *The delivery of free molecules into the cytoplasm and nucleus by using arginine-rich cell-penetrating peptides (CPPs) has been limited to small cargoes, while large cargoes such as proteins are taken up and trapped in endocytic vesicles. Based on recent work, in which we showed that the transduction efficiency of arginine-rich CPPs can be greatly enhanced by cyclization, the aim was to use cyclic CPPs to transport full-length proteins, in this study green fluorescent protein (GFP), into the cytosol of living cells. Cyclic and linear CPP–GFP conjugates were obtained by using azido-functionalized CPPs and an alkyne-functionalized GFP. Our findings reveal that the cyclic-CPP–GFP conjugates are internalized into live cells with immediate bioavailability in the cytosol and the nucleus, whereas linear CPP analogues do not confer GFP transduction. This technology expands the application of cyclic CPPs to the efficient transport of functional full-length proteins into live cells.*

Arginine-rich cell-penetrating peptides (CPPs) have the ability to cross into cells and transport other molecular cargoes in a non-endocytic manner.[1] This mode of cellular delivery, hereafter referred to as transduction, offers immediate free access to the cytoplasm and nucleus, thus making it ideal for the transport of drugs and biomarkers.[2] The transduction efficiency is, however, limited by the size of the cargo,[3] which has confined the application of CPPs to the non-endocytic delivery of small cargoes, such as fluorophores or small to medium-sized peptides. By contrast, proteins coupled to linear CPPs are taken up largely into cytoplasmic vesicles, which leads to endosomal trapping and lysosomal degradation with little or no access to intracellular targets. Great effort has been invested into trying to overcome this barrier and deliver full-length proteins into living cells by using CPPs. Earlier studies reported the delivery of an arginine-rich green fluorescent protein (GFP) fusion, which apparently resulted in free intracellular GFP.[4] However, these results were subsequently shown to be a consequence of fixation artifacts.[5] More recent reports on arginine-substituted supercharged GFP have shown cellular uptake, but the protein was trapped in endocytic vesicles.[6] Alternative approaches for protein delivery include physical disruption of the plasma membrane by electroporation or microinjection and the use of delivery additives.[7] In this study, we employed chemoselective conjugation strategies to attach synthetic CPPs to facilitate passive intracellular protein delivery. This approach minimizes cellular stress and thus holds great potential for pharmaceutical applications. Recently, we discovered that the transduction efficiency of arginine-rich peptides, such as the TAT peptide,[8] can be greatly enhanced by employing cyclic analogues.[9] More specifically, we showed that the cyclization of arginine-rich peptides significantly increases the speed at which these peptides enter living cells. However, it remained an open question whether, besides an increase in kinetic efficiency, cyclization also enables the transport of larger cargoes in a non-endocytic manner, thus overcoming the cargo size limit for transduction.[3] Therefore, we investigated whether this simple structural modification of the peptide enables the transduction of full-length proteins. GFP is a frequently used model protein for probing cellular protein uptake because its intracellular distribution in living cells can be immediately detected by using live-cell confocal microscopy. Moreover, the fluorescence of GFP indicates correct folding of the protein structure. Herein, we show that after conjugating GFP to a cyclic TAT CPP, the protein is delivered into living cells and is immediately free in the cytosol and nucleus.

To access a site-specific cyclic TAT–GFP conjugate (**cTAT-GFP**; Figure 1b), we applied the chemoselective

[*] N. Nischan,[+] Prof. C. P. R. Hackenberger[+]
Leibniz-Institut für Molekulare Pharmakologie (FMP)
Robert-Rössle-Strasse 10, 13125 Berlin (Germany)
E-mail: hackenbe@fmp-berlin.de
N. Nischan[+]
Freie Universität Berlin, Institut für Chemie und Biochemie
Takustrasse 3, 14195 Berlin (Germany)
Dr. H. D. Herce,[+] Dr. F. Natale, Prof. M. C. Cardoso[+]
Technische Universität Darmstadt, Fachbereich Biologie
Schnittspahnstrasse 10, 64287 Darmstadt (Germany)
E-mail: Cardoso@bio.tu-darmstadt.de
Dr. H. D. Herce[+]
Department of Physics, Applied Physics, and Astronomy
Rensselaer Polytechnic Institute
110 Eighth Street, Troy, NY, 12180 (United States)
N. Bohlke, Prof. N. Budisa
Technische Universität Berlin, Institut für Chemie
Müller-Breslau-Str. 10, 10623 Berlin (Germany)
Prof. C. P. R. Hackenberger[+]
Humboldt Universität zu Berlin, Department Chemie
Brook-Taylor-Strasse 2, 12489 Berlin (Germany)
[+] These authors contributed equally.

[**] This work was funded by the Deutsche Forschungsgemeinschaft (SPP1623, Teilprojekt Prof. Cardoso/ Prof. Hackenberger/ Prof. Leonhardt, SFB765 B5), the Fonds der Chemischen Industrie, and the Boehringer-Ingelheim Foundation (Plus 3 award). We also thank Anne Lehmkuhl for excellent technical support.

Supporting information for this article is available on the WWW under http://dx.doi.org/10.1002/anie.201410006.

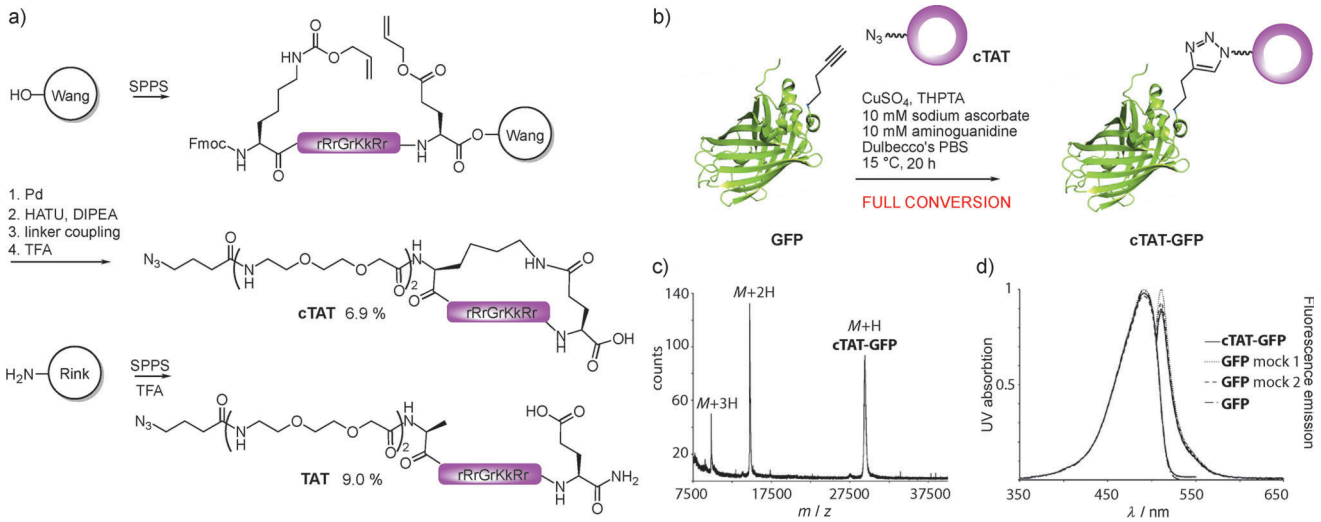

Figure 1. Synthesis of conjugatable cyclic and linear TAT-derived CPPs and conjugation with **GFP**. a) Synthesis of the peptides **cTAT** and **TAT**. b) CuAAC of alkyne-GFP and **cTAT** under optimized conditions to yield **cTAT-GFP**. c) MALDI spectrum of the reaction product after dialysis. d) Absorption and fluorescence emission (excitation at 495 nm) of **cTAT-GFP**, untreated **GFP**, and **GFP** treated with all reagents except azide (**GFP** mock 1) or no reagents (**GFP** mock 2). Each set of graphs was normalized to the graph with the highest intensity.

copper-catalyzed azide–alkyne cycloaddition (CuAAC)[10]. A cyclic azido-TAT peptide (**cTAT**) was reacted with a GFP mutant, obtained through auxotrophic expression in *E. coli*,[11] that carries a homopropargyl glycine at the N terminus (see the Supporting Information). The use of chemoselective protein modification techniques[12] is essential not only for control of the conjugation site but also since cyclic peptides cannot be introduced by standard protein biosynthesis. The cyclic CPP for the later uptake experiments was designed to contain a highly positively charged TAT sequence of alternating L and D amino acids for maximal uptake efficiency[9] and a flexible spacer region carrying the reactive azido group at a reasonable distance to facilitate effective conjugation and flexible presentation of the peptide.

The cyclic TAT peptide was synthesized on a standard Wang resin with orthogonal protecting groups at Lys and Glu for cyclization on the solid support (Figure 1a). Initially, we used a short five amino acid peptide (GKGNG) as a spacer and either azido benzoic acid or azido butanoic acid at the N terminus. The corresponding peptides were obtained in 3–4% overall yield (see the Supporting Information).

However, despite optimization efforts, these CPPs resulted only in incomplete conversions in the later CuAAC conjugation studies (Figures S6, S7 in the Supporting Information). Moreover, the separation of **GFP** and the conjugation product was not successful. However, a cyclic TAT peptide with an N-terminal azide and an oligoethylene glycol spacer (**cTAT**, Figure 1a) could be isolated in spite of its extreme hydrophilicity and in only one purification step through reversed phase HPLC at reduced flow rate in an overall yield of 6.9%. Most importantly, this azido-peptide building block also demonstrated superior results in terms of conjugation to the alkyne-GFP. For the CuAAC, we started with a general method[10c] previously employed for the glycosylation of alkyne-containing proteins in our group[13] and optimized it for the conjugation of **GFP** and **cTAT**. We found that full conversion and good recovery is reached reproducibly at 15 °C in 20 h (Figure 1b,c). Purification of the protein with optimal recovery was achieved by performing dialysis against EDTA in Dulbecco's PBS, followed by HEPES buffer.

As an additional control, we synthesized a linear TAT–GFP conjugate (**TAT-GFP**) through an analogous synthetic strategy to probe the impact of cyclization of the TAT sequence on cellular uptake (see Figure 1a and the Supporting Information). The linear **TAT** peptide is the equivalent of **cTAT** in terms of stereochemistry and linker design; minor changes include an alanine to reflect the cyclized lysine and a glutamic acid with a C-terminal amide instead of a carboxylic acid to maintain overall charge and proteolytic stability of the C terminus. Nonconjugated **GFP** that underwent the same chemical procedures as the CPP-conjugated variants was used as a negative control in the uptake experiments.

To verify that the conjugation has no influence on the photophysical properties of GFP, we compared the UV-absorption and fluorescence spectra (Figure 1d) of isolated **cTAT-GFP** to those of **GFP** protein samples exposed to an identical procedure but either without the azide group (**GFP** mock 1) or with no reagents (**GFP** mock 2), as well as **GFP** that was only subjected to the workup. At similar protein concentrations, all of the tested proteins showed equal absorbance maxima at 495 nm, as well as fluorescence emission maxima at 509 nm with similar intensities (Figure S12–14).

At the outset of our cell uptake studies, we illustrated our desired mode of cellular uptake (transduction) by comparing the uptake of a linear TAT–fluorophore conjugate to that of an amphipathic fluorescently labeled control peptide (PTD4; see the Supporting Information for the conditions).[1a,2a,b] Although both peptides have affinity for the plasma membrane, while the PTD4 gets trapped in endosomes, the TAT-conjugated peptide is successfully delivered into the cell and

can be found freely distributed throughout the cell (Figure S15).

We then compared the cellular uptake and intracellular distribution of **cTAT-GFP**, **TAT-GFP**, and unconjugated **GFP** by performing live-cell confocal microscopy in a human cervical cancer cell line (HeLa). The cells were incubated with the proteins for 40 min in HEPES buffer lacking nutrients and glucose to reduce endocytosis at the concentrations indicated, imaged (Figure S16), and finally washed and imaged again (Figure 2). For quantification of the transduction efficiency, all cells showing homogenous staining of cytoplasm and nucleoli were considered positive. The results show that unconjugated **GFP** at 150 μM was not taken up by living cells (Figure 2a). We also added rhodamine-labeled TAT CPP at 5 μM concentration to the unconjugated **GFP** solution (Figure 2b). While the TAT CPP was taken up into most of the cells and accumulated in the cytosol and nucleolus at high levels, the unconjugated **GFP** at 30-fold higher concentration was not internalized by the cells. Next, we tested the cellular uptake efficiency of the linear **TAT-GFP** conjugate at different concentrations (50, 100 and 150 μM). We detected very low intracellular **GFP** signal, even at the highest concentration used (150 μM); only 1% of the cells were transduced (Figure 2c,e), which is in accordance with our previous observations.[3] No uptake was detected at 50 and 100 μM. By contrast, **cTAT-GFP** was efficiently taken up by most of the living cells at all concentrations tested (50–150 μM; Figure 2d,e). In our earlier observations with cyclic TAT peptide versus linear TAT peptide, we found that the larger arginine side chain separation in cyclic TAT increased the uptake efficiency and kinetics.[9] The data presented herein show that this structural modification can also be exploited for the delivery of much larger cargoes, in this case a fully folded 27.5 kDa protein.

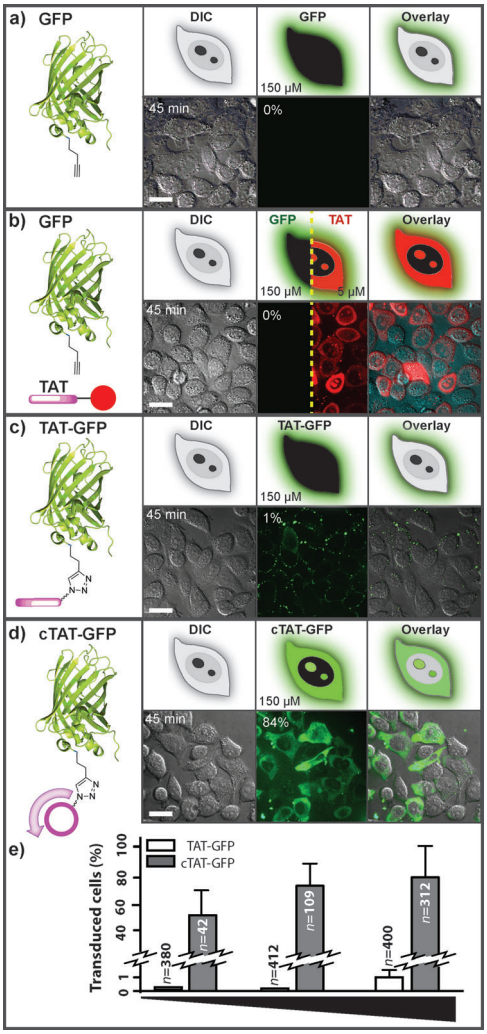

Figure 2. Chemoselective conjugation of **GFP** to cyclic **cTAT** enables the transduction of living cells. a) **GFP** added to the extracellular media was not taken up by living cells. b) While the TAT peptide was able to efficiently enter living cells, unconjugated **GFP** remained excluded from the cells. c) Conjugation of linear **TAT** to **GFP** (**TAT-GFP**) does not lead to efficient transduction; at 150 μM, only 1% of the cells contained **TAT-GFP**. d) **cTAT-GFP** efficiently entered living cells. e) Quantification of the percentage of transduced cells for 50, 100 and 150 μM of **TAT-GFP** and **cTAT-GFP**. Cells were scored as positive when showing a diffuse cytoplasmic and nucleolar fluorescence signal. Error bars: standard deviation. Scale bar: 15 μm.

Notably, as indicated by fluorescence recovery after photobleaching (FRAP) experiments, the protein **cTAT-GFP** was freely distributed throughout the cell cytoplasm and nucleus (Figure S17). In particular, the nuclear localization of **GFP** indicates non-endocytic uptake. To further test this mode of entry, we studied the uptake of **cTAT-GFP** in the presence of a macropinocytosis inhibitor and at 4°C (Figure S18), and the results show that the mode of uptake is energy independent.

Upon comparison of intracellular fluorescence relative to extracellular fluorescence before washing, we found that the intracellular concentration of rhodamine-labeled TAT was much higher than the extracellular concentration, whereas the protein conjugate **cTAT-GFP** showed the opposite relationship (Figure S16b,c). We attribute this observation to the significant size difference between a 2 kDa peptide and a 27.5 kDa protein. An estimate of the GFP intracellular concentration is shown in Figure S19. The general morphology of the cells and the fact that the cells continue to move and undergo mitotic division (movie 1) indicates that **cTAT-GFP** uptake is well tolerated and does not interfere with cell integrity or metabolism.

In summary, we have shown that the chemoselective conjugation of cyclic cell-penetrating peptides to alkyne-GFP gives access to full-length folded GFP conjugates, which are taken up into live cells with immediate cytosolic and nuclear availability. Since the incorporation of alkyne groups into proteins is well established, this technology is generally applicable to the production of other transducing proteins with comparable size. This covalent approach offers multiple strategies to further optimize the transduction efficiency of full-length proteins depending on the particular application, such as the coupling of multiple CPPs to a single protein, the exploration of other CPPs such as cyclic R10,[9] and combination with other protein delivery strategies such as electroporation or the use of delivery additives[7]. While these avenues need to be explored to further increase protein uptake under growth conditions and for therapeutic applica-

tions, our results demonstrate remarkably efficient and direct cytosolic delivery of a folded full-length functional protein covalently coupled to a cyclic arginine-rich peptide. This method opens new venues for the application of proteins, for example, in cell screenings.

Experimental Section

Peptide Synthesis: All peptides were synthesized by using solid-phase peptide synthesis and characterized by HPLC-UV or UPLC-UV, as well as high resolution ESI-MS. For detailed synthesis protocols and analytical data for **cTAT** and **TAT**, see the Supporting Information. Details on **TAT-FITC**, **TAT-TAMRA**, and **PTD4-TAMRA** peptides can be found in Ref. [9].

Expression and Purification of HPG-GFP: The plasmid pET30b GFPhs1-RM, which encodes a mutated variant of GFP containing only the N-terminal methionine (Met; GFPhs1-RM,[14] 245 amino acids, 27.6 kDa) was kindly provided by Soundrarajan Nagasundarapandian from the group of Prof. Sun Gu Lee (Pusan University, South Korea). A Tobacco Etch Virus (TEV) protease recognition site was introduced for removal of the C-terminal His-tag. Glutamine at the N-terminus ensures that the N-terminal Met or homopropargylglycine (HPG) is not cleaved. For expression of GFPhs1-RM TEV, the Met auxotrophic *E. coli* strain B834 (DE3) [B→B834[15]→B834 (DE3)][16] was transformed with pET30b GFPhs1-RM TEV. Expression was carried out under a final HPG concentration of 50 mg mL^{-1}. After cell lysis, HPG-GFP (**GFP**) was immobilized on a Ni-NTA column and cleaved by using TEV protease.

CPP–GFP Conjugation: Mutant **GFP** was conjugated with **cTAT** or **TAT** peptides by using CuAAC. Optimized reaction conditions include shaking with 1,000 turns per minute at 15 °C for 20 h in Ca/Mg-free Dulbecco's phosphate-buffered saline (PBS) at final concentrations of 20 μM protein, 500 μM azidopeptide, 200 μM $CuSO_4$, 1 mM THPTA ligand, and 10 mM aminoguanidine hydrochloride and sodium ascorbate; batch size 500 μL. The reaction was quenched with 50 μL of 5 mM EDTA. The copper was removed through dialysis against 2.5 mM EDTA in Ca/Mg-free Dulbecco's PBS, and then the EDTA was removed through dialysis against HEPES buffer. Full conversion and formation of the product was verified through MALDI-TOF.

Cellular uptake experiments were performed as described elsewhere[9] with minor changes. Briefly, cells were washed twice with Ca^{2+}-free medium (without serum) and the peptides were added. Peptides or (un)conjugated GFP proteins were diluted to different concentrations in a buffer (140 mM NaCl, 2.5 mM KCl, 5 mM HEPES, 5 mM glycine, pH value adjusted with NaOH) and incubated with cells for 60 min at 37 °C in optically proficient glass-bottom multiwell chambers (total sample volumes: 30 μL). Subsequently, the peptide solution was gently exchanged with growth medium and the cells were imaged.

Confocal Microscopy and Image Analysis: Imaging was carried out with an UltraVIEWVoX spinning disc confocal system (Perkin-Elmer, UK). Cells were imaged in a closed live cell microscopy chamber (ACU control, Olympus, Japan) heated to 37 °C, with 5 % CO2 and 60 % air humidity, mounted on a Nikon Ti microscope (Nikon, Japan). Image acquisition was performed with a × 60/1.45 NA Planapochromat oil immersion objective lens. Images were obtained with a cooled 14-bit EMCCD camera (C911-50, CamLink). To visualize the GFP signal, a 488 nm excitation laser and a 521 nm emission filter were used. TAMRA was excited by using a 561 nm laser and the emission was filtered through a 587 nm filter. For transduction efficiency calculations, the cells showing homogenous staining of the cytoplasm and nucleoli were considered positive.

Received: October 12, 2014
Published online: December 17, 2014

Keywords: cell-penetrating peptides · click chemistry · cyclic peptides · live-cell microscopy · protein delivery

[1] a) G. Ter-Avetisyan, G. Tunnemann, D. Nowak, M. Nitschke, A. Herrmann, M. Drab, M. C. Cardoso, *J. Biol. Chem.* **2009**, *284*, 3370 – 3378; b) F. Duchardt, M. Fotin-Mleczek, H. Schwarz, R. Fischer, R. Brock, *Traffic* **2007**, *8*, 848 – 866; c) H. D. Herce, A. E. Garcia, M. C. Cardoso, *J. Am. Chem. Soc.* **2014**, DOI: 10.1021/ja507790z.

[2] a) R. Brock, *Bioconjugate Chem.* **2014**, *25*, 863 – 868; b) S. Futaki, H. Hirose, I. Nakase, *Curr. Pharm. Des.* **2013**, *19*, 2863 – 2868; c) H. D. Herce, W. Deng, J. Helma, H. Leonhardt, M. C. Cardoso, *Nat. Commun.* **2013**, *4*, 2660 – 2667.

[3] G. Tunnemann, R. M. Martin, S. Haupt, C. Patsch, F. Edenhofer, M. C. Cardoso, *Faseb J.* **2006**, *20*, 1775 – 1784.

[4] N. J. Caron, Y. Torrente, G. Camirand, M. Bujold, P. Chapdelaine, K. Leriche, N. Bresolin, J. P. Tremblay, *ASGT Mol. Therapy* **2001**, *3*, 310 – 318.

[5] J. P. Richard, K. Melikov, E. Vives, C. Ramos, B. Verbeure, M. J. Gait, L. V. Chernomordik, B. Lebleu, *J. Biol. Chem.* **2003**, *278*, 585 – 590.

[6] a) S. M. Fuchs, R. T. Raines, *ACS Chem. Biol.* **2007**, *2*, 167 – 170; b) B. R. McNaughton, J. J. Cronican, D. B. Thompson, D. R. Liu, *Proc. Natl. Acad. Sci. USA* **2009**, *106*, 6111 – 6116.

[7] a) K. Inomata, A. Ohno, H. Tochio, S. Isogai, T. Tenno, I. Nakase, T. Takeuchi, S. Futaki, Y. Ito, H. Hiroaki, M. Shirakawa, *Nature* **2009**, *458*, 106 – 109; b) T. Takeuchi, M. Kosuge, A. Tadokoro, Y. Sugiura, M. Nishi, M. Kawata, N. Sakai, S. Matile, S. Futaki, *ACS Chem. Biol.* **2006**, *1*, 299 – 303.

[8] A. D. Frankel, C. O. Pabo, *Cell* **1988**, *55*, 1189 – 1193.

[9] G. Lättig-Tünnemann, M. Prinz, D. Hoffmann, J. Behlke, C. Palm-Apergi, I. Morano, H. D. Herce, M. C. Cardoso, *Nat. Commun.* **2011**, *2*, 453 – 464.

[10] a) C. W. Tornøe, C. Christensen, M. Meldal, *J. Org. Chem.* **2002**, *67*, 3057 – 3064; b) V. V. Rostovtsev, L. G. Green, V. V. Fokin, K. B. Sharpless, *Angew. Chem. Int. Ed.* **2002**, *41*, 2596 – 2599; *Angew. Chem.* **2002**, *114*, 2708 – 2711; c) V. Hong, S. I. Presolski, C. Ma, M. G. Finn, *Angew. Chem. Int. Ed.* **2009**, *48*, 9879 – 9883; *Angew. Chem.* **2009**, *121*, 10063 – 10067; d) B. T. Worrell, J. A. Malik, V. V. Fokin, *Science* **2013**, *340*, 457 – 460.

[11] a) N. Budisa, *Angew. Chem. Int. Ed.* **2004**, *43*, 6426 – 6463; *Angew. Chem.* **2004**, *116*, 6586 – 6624; b) L. Wang, P. G. Schultz, *Angew. Chem. Int. Ed.* **2005**, *44*, 34 – 66; *Angew. Chem.* **2005**, *117*, 34 – 68.

[12] a) K. Lang, J. W. Chin, *ACS Chem. Biol.* **2014**, *9*, 16 – 20; b) C. P. R. Hackenberger, D. Schwarzer, *Angew. Chem. Int. Ed.* **2008**, *47*, 10030 – 10074; *Angew. Chem.* **2008**, *120*, 10182 – 10228; c) D. Schumacher, C. P. R. Hackenberger, *Curr. Opin. Chem. Biol.* **2014**, *22*, 62 – 69.

[13] L. M. Artner, L. Merkel, N. Bohlke, F. Beceren-Braun, C. Weise, J. Dernedde, N. Budisa, C. P. R. Hackenberger, *Chem. Commun.* **2012**, *48*, 522 – 524.

[14] S. Nagasundarapandian, L. Merkel, N. Budisa, R. Govindan, N. Ayyadurai, S. Sriram, H. Yun, S. G. Lee, *ChemBioChem* **2010**, *11*, 2521 – 2524.

[15] W. B. Wood, *J. Mol. Biol.* **1966**, *16*, 118 – 133.

[16] a) F. W. Studier, P. Daegelen, R. E. Lenski, S. Maslov, J. F. Kim, *J. Mol. Biol.* **2009**, *394*, 653 – 680; b) F. W. Studier, B. A. Moffatt, *J. Mol. Biol.* **1986**, *189*, 113 – 130.

Angewandte Chemie
Eine Zeitschrift der Gesellschaft Deutscher Chemiker

Supporting Information

69451 Weinheim, Germany

Covalent Attachment of Cyclic TAT Peptides to GFP Results in Protein Delivery into Live Cells with Immediate Bioavailability**

Nicole Nischan, Henry D. Herce, Francesco Natale, Nina Bohlke, Nediljko Budisa, M. Cristina Cardoso, and Christian P. R. Hackenberger**

anie_201410006_sm_miscellaneous_information.pdf
anie_201410006_sm_movie_mitosis.mov

C

SUPPORTING INFORMATION

Table of Contents

1 Abbreviations used S2

2 Synthesis Conjugatable Peptides S3

2.1 General Information S3

2.2 Synthesis of **cTAT** S3

2.3 Synthesis of cyclic TAT peptides with peptide linker S4

2.4 Synthesis of **TAT** S6

3 Protein Biosynthesis S8

3.1 Strains and Plasmids S8

3.2 Protein Biosynthesis and Purification S8

4 Protein-Peptide Conjugation S10

4.1 Optimized Procedure S10

4.2 Initial efforts on getting access to pure CPP-GFP conjugates S10

4.3 Representative MALDI Spectra of **GFP**, **cTAT-GFP** and **TAT-GFP** S12

4.4 Photophysical Properties of **GFP** and **cTAT-GFP** S13

5 Cellular Uptake S16

5.1 Cellular Uptake by Transduction Versus Endocytosis S16

5.2 Live Cell Confocal Microscopy of Transduced Cells S16

5.3 Fluorescence Recovery After Photobleaching of Internalized GFP S17

5.4 Cellular Uptake Does Not Require Macropinocytosis or Metabolic Energy S18

5.5 Quantification of GFP Intracellular Concentration S20

5.6 Movie of Transduced Cells – Motility and Mitosis S21

6 References S22

7 Appendix S23

1 Abbreviations used

AcOH	acetic acid
Alloc	allyloxycarbonyl-
CuAAC	Copper(I)-catalyzed Azide-Alkyne Cycloaddition
DHAP	dihydroxyacetone phosphate
DIC	diisopropylcarbodiimide
DIC	differential interference contrast microscopy
DIPEA	N,N-diisopropylethylamine
DMF	dimethylformamide
DTT	dithiothreitol
EDTA	ethylenediaminetetraacetic acid
Eq.	equivalents
ESI-MS	electrospray ionization mass spectrometry
FA	formic acid
FI	fluorescence intensity
Fmoc	fluorenylmethyloxycarbonyl-
HATU	1-[bis(dimethylamino)methylene]-1*H*-1,2,3-triazolo[4,5-b]pyridinium 3-oxid hexafluorophosphate
HBTU	*N*,*N*,*N*',*N*'-Tetramethyl-*O*-(1*H*-benzotriazol-1-yl)uronium hexafluorophosphate
HEPES	2-[4-(2-hydroxyethyl)piperazin-1-yl]ethanesulfonic acid
HOBt	1-hydroxybenzotriazole
HPLC	high-performance liquid chromatography
MALDI	Matrix-assisted laser desorption/ionization
MeCN	acetonitrile
NMM	4-methylmorpholine 4-oxide
OAll	Allyloxy-
PBS	phosphate buffered saline
ROI	region of interest
TFA	trifluoroacetic acid
THPTA	Tris(3-hydroxypropyl triazolylmethyl)amine
TIS	triisopropylsilane
UPLC	ultra performance liquid chromatography
UV	ultraviolet

2 Synthesis Conjugatable Peptides

2.1 General Information

Reagents and solvents, unless stated otherwise, were commercially available as reagent grade or HPLC grade and did not require further purification. Amino acids were purchased from IRIS Biotech GmbH (Germany), resins from Novabiochem (Merck KGaA, Germany).
SPPS. Peptides were synthesized with an Activo-P11 Peptide Synthesizer (Activotec SPP Ltd., UK) via standard Fmoc-based conditions using HOBt/HBTU/DIPEA activation and piperidine Fmoc deprotection in DMF.
HPLC-UV purity of peptides was determined at 220 nm using a system consisting of a Waters 600S controller, a Waters 616 pump, a Waters 717plus autosampler and a Waters 2489 UV/Visible detector (all Waters Corporation, US) on a C18-column (Eclipse, Agilent Technologies, USA) at constant flow of 1.0 mL/min of 0 % to 50 % acetonitrile in water (with 0.1 % TFA) over 30 min.
High-resolution mass spectra (HRMS) were either collected with a Waters Acquity UPLC coupled to an LCT Premier Micromass Technologies System using as an eluent water and MeCN containing 0.1 % formic acid at a flow rate of 0.2 mL/min on a C18 column. The data was processed using Mass Lynx Software (all Waters Corporation, US). Alternatively, ESI-MS was measured on an Agilent 6210 ToF LC-MS system (Agilent Technologies, US) at constant flow of 0.2 mL/min with water and MeCN containing 1 % FA to give high resolution mass spectra.

2.2 Synthesis of cTAT

Scheme S1. Synthesis of conjugatable cyclic TAT peptide (**cTAT**).

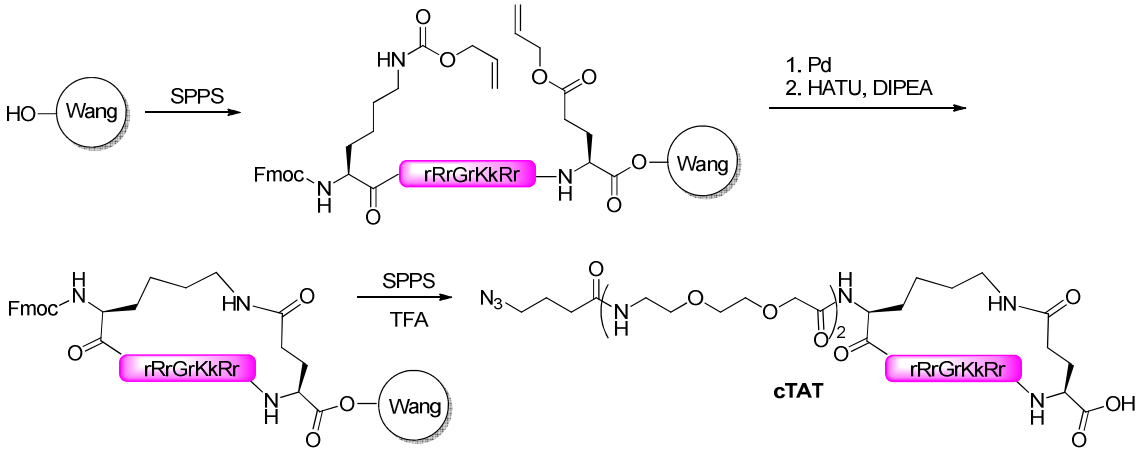

First, a linear peptide of the sequence (Fmoc)(Alloc)KrRrGrKkRr(OAll)Q was synthesized on a Wang resin (0.25 mmol, 0.22 mmol/g). Upper case letters correspond to L-, lower case letters to D-amino acids. The first amino acid, Fmoc-(allyl)glutamic acid, was loaded manually. Other couplings were performed using double couplings of 10 eq. of amino acid The N-terminal Fmoc was left on the peptide.
The Alloc and OAll protecting groups were removed using $Pd(PPh_3)_4$(270 mg, 0.5 eq.) in a mixture of $CHCl_3$/AcOH/NMM in a ratio of 37/2/1 for two hours at room temperature under Argon bubble mixture. To remove the Palladium catalyst afterwards, it was additionally washed with 0.2 M DIPEA in DMF. Then the peptide was cyclized using two equivalent of HATU/DIPEA in DMF for two hours, followed by capping. After Fmoc removal a linker consisting of two repeats of [2-[2 -aminoethoxy]ethoxy]acetic acid was introduced and azidobutanoic acid was coupled to the N-terminus of this linker. These couplings were each performed twice using 5 eq. of HOBt/DIC activated acid in DMF.

After washing and drying the peptide was cleaved from the solid support (two hours in 8 mL of mixture 95 % TFA, 2 % TIS, 2 % DTT, 1 % MeSPh) and precipitated in 100 mL of diethylether. The peptide was isolated using preparative HPLC (gradient 0 to 40 % in 100 min of B in A, A being 100 % water, B being 100 % MeCN, each containing 0.1 % TFA on a RP-C18 column (Nucleodur C18 HTec (Machenerey Nagel, Germany), 100 Å, 5 µm, 250 mm x 32 mm, 17 mL/min)) to yield in a white trifluoroacetate (48.92 mg, 17.35µmol, yield 6.9 %, molar mass (peptide) = 1.91 kDa, molar mass (TFA_8 salt) = 2.82 kDa) in good purity. HRMS: m/z: 382.6376 $[M+5H]^{5+}$ (calcd. m/z: 382.6375, Δ 0.3 ppm), see appendix for spectra.

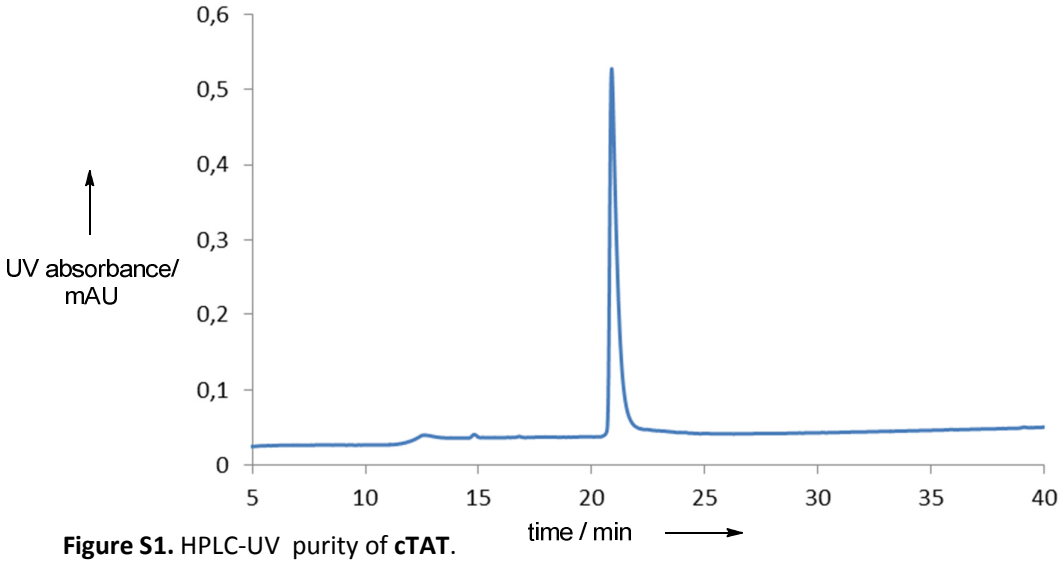

Figure S1. HPLC-UV purity of **cTAT**.

2.3 Synthesis of cyclic TAT peptides with peptide linker

Cyclic TAT with GKGNG-linker functionalized with azidobenzoic acid

Scheme S2. Synthesis of conjugatable cyclic TAT peptide with GKGNG-linker functionalized with azidobenzoic acid (**cTAT A**).

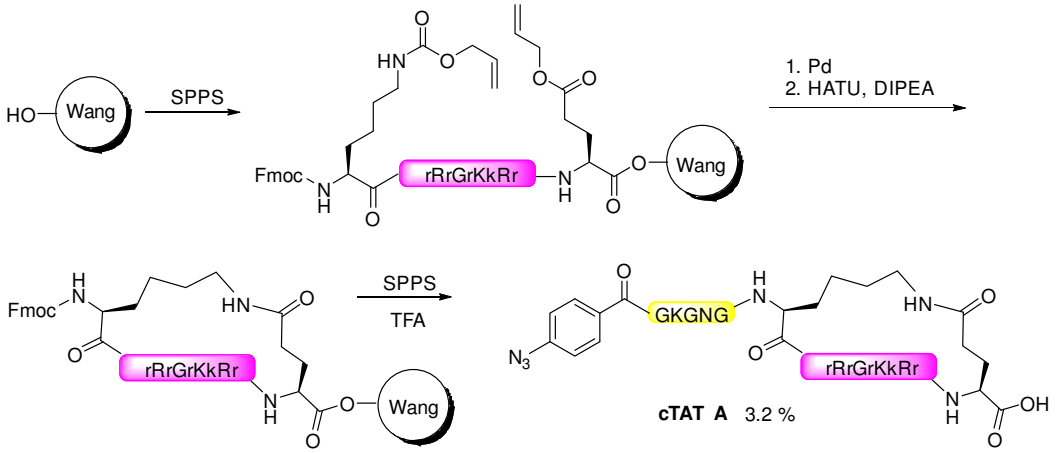

Wang resin (0.1 mmol, 0.20 mmol/g) was loaded with Fmoc-(allyl)glutamic acid and applied to SPPS using double couplings and capping with HOBt/HBTU/DIPEA in NMP on the Applied Biosystem synthesizer for the first nine standard amino acids (sequence = rRrGrKkRr) and Alloc-protected lysine. After that, Allyl-protected glutamic acid and Alloc-protected lysine were deprotected using $Pd(PPh_3)_4$ in a mixture of $CHCl_3$/ AcOH/ NMM in a ratio of 37/ 2/ 1 for two hours at room temperature.

Afterwards the peptide was cyclized on the solid support using one equivalent of HATU and two equivalents of DIPEA. Then the linker (GKGNG) was attached to the peptide via SPPS using double couplings with HOBt/DIC in DMF manually. At the N-terminus, *para*-azidobenzoic acid was coupled (10 eq., 2 x 2h, RT, HOBt and DIC in DMF). After washing and drying, the peptide was cleaved from the solid support (2 h in 2 ml of mixture 95 % TFA, 2 % TIS, 2 % DTT, 1 % MeSPh) and purified by semi-preparative HPLC (0 to 50 % of MeCN in Water, containing 0.1 % TFA on RP-C18 column) to yield in a white trifluoroacetate (9.83 mg, 3.18 µmol, yield 3.2 %, molar mass (peptide) = 2.06 kDa, molar mass (TFA_9 salt) = 3.09 kDa) in good purity. HRMS: m/z: 517.3029 $[M+4H]^{4+}$ (calcd. m/z: 517.3042), see appendix for spectra.

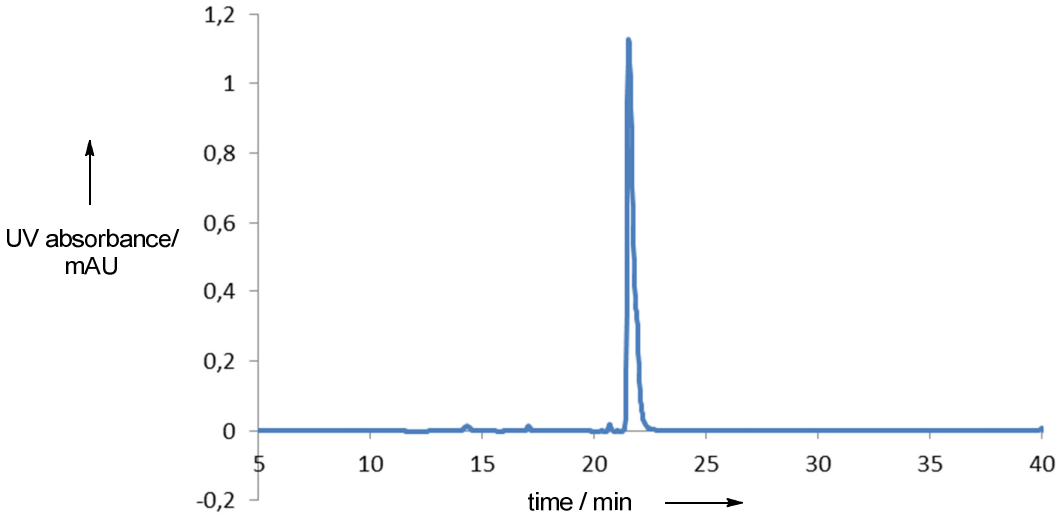

Figure S2. HPLC-UV purity of **cTAT A**.

Cyclic TAT with GKGNG-linker functionalized with azidobutanoic acid

Scheme S3. Synthesis of conjugatable cyclic TAT peptide with GKGNG-linker functionalized with azidobutanoic acid (**cTAT B**).

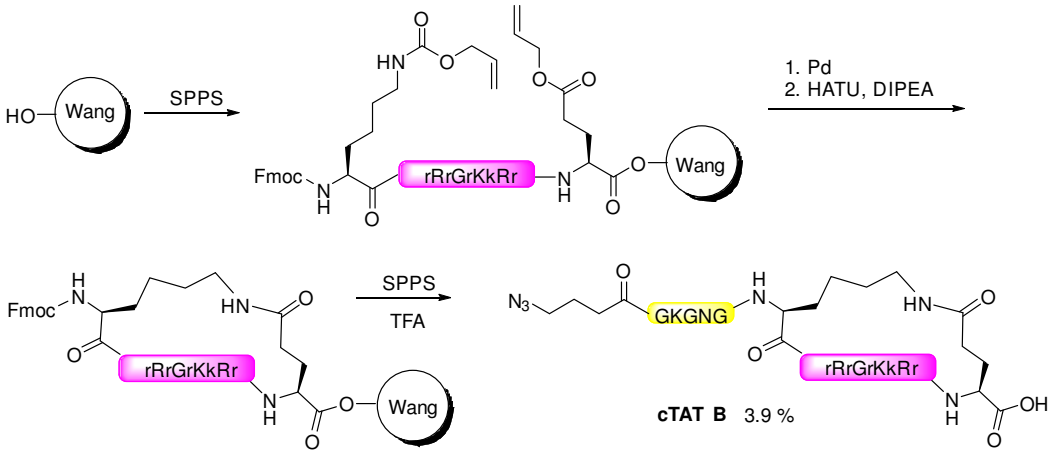

Wang resin (0.05 mmol, 0.22 mmol/g) was loaded with Fmoc-(allyl)glutamic acid and applied to SPPS using double couplings and capping with HOBt/HBTU/DIPEA in NMP on the Applied Biosystem synthesizer for the first nine standard amino acids (sequence = rRrGrKkRr) and Alloc-protected lysine. After that, allyl-protected glutamic acid and Alloc-protected lysine were deprotected using $Pd(PPh_3)_4$ in a mixture of $CHCl_3$/ AcOH/ NMM in a ratio of 37/ 2/ 1 for two hours at room temperature. Afterwards the peptide was cyclized on the solid support using one equivalent of HATU and two equivalents of DIPEA. Then the linker (GKGNG) was attached to the peptide via SPPS using double

couplings with HOBt/DIC in DMF manually. At the N-terminus, azidobutanoic acid was coupled (20 eq., 2h, RT, HATU and DIPEA in DMF). After washing and drying, the peptide was cleaved from the solid support (2 h in 3 ml of mixture 95 % TFA, 2 % TIS, 2 % DTT, 1 % MeSPh) and purified by semi-preparative HPLC (0.8 to 32 % of MeCN in Water containing 0.1 % TFA over 70 min on a RP-C18 column (100 Å 5 µ, 21 mm x 250 mm) at a flow of 5 mL/min) to yield in a white trifluoroacetate (5.94 mg, 1.94 µmol, yield 3.9 %, molar mass (peptide) = 2.03 kDa, molar mass (TFA_9 salt) = 3.06 kDa) in good purity. HRMS: m/z: 678.0753 $[M+3H]^{3+}$ (calcd. m/z: 678.0748), see appendix for spectra.

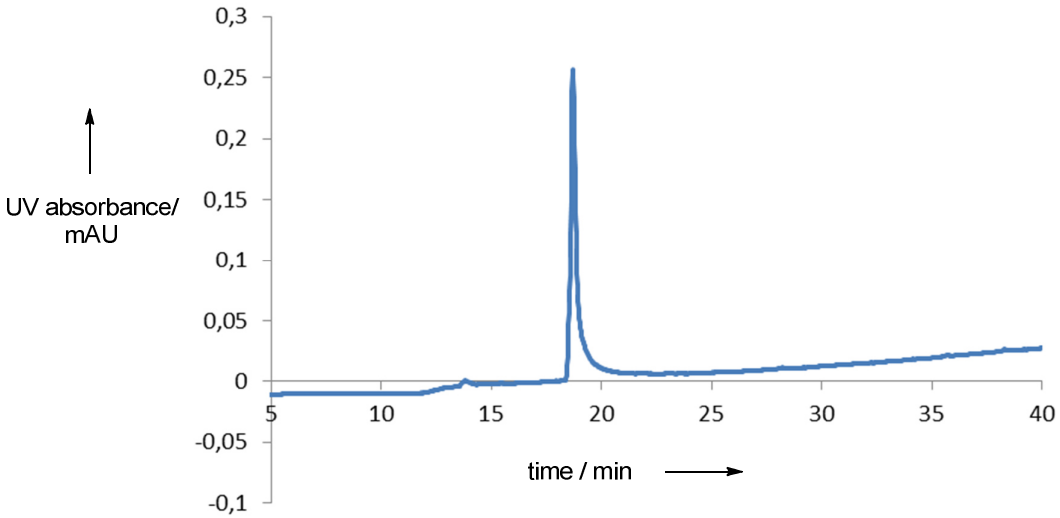

Figure S3. HPLC-UV purity of **cTAT B**.

2.4 Synthesis of TAT

Scheme S4. Synthesis of conjugatable linear TAT peptide (**TAT**).

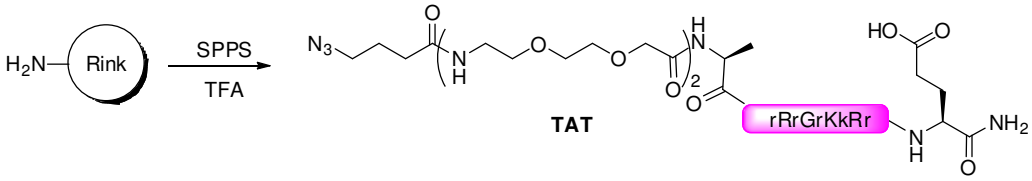

The linear control peptide ArRrGrKkRrQ was synthesized on Rink amide resin (0.1 mmol, 0.71 mmol/g) using double couplings of 5 eq. of amino acid. Upper case letters correspond to L-, lower case letters to D-amino acids. To the N-terminus, a linker consisting of two repeats of [2-[2 -aminoethoxy]ethoxy]acetic acid and finally azidobutanoic acid was coupled. These couplings were each performed twice using 5 eq. of HOBt/DIC activated acid in DMF.

After washing and drying the peptide was cleaved from the solid support (two hours in 3 ml of mixture 95 % TFA, 2 % TIS, 2 % DTT, 1 % MeSPh), precipitated in 100 mL of diethylether. The peptide was isolated using preparative HPLC (5 to 50 % of B in A, A being 100 % water, B being 80 % MeCN in water, each containing 0.1 % TFA on a RP-C18 column (100 Å, 5 µm, 250 mm x 20 mm, 5 mL/min) to yield in a white trifluoroacetate (25.06 mg, 9.02 µmol, yield 9,0 %, molar mass (peptide) = 1,87 kDa, molar mass (TFA_8 salt) = 2,78 kDa) in good purity. HRMS: m/z: 374.6313 $[M+5H]^{3+}$ (calcd. m/z: 374.6309, Δ 1.1 ppm), see appendix for spectra.

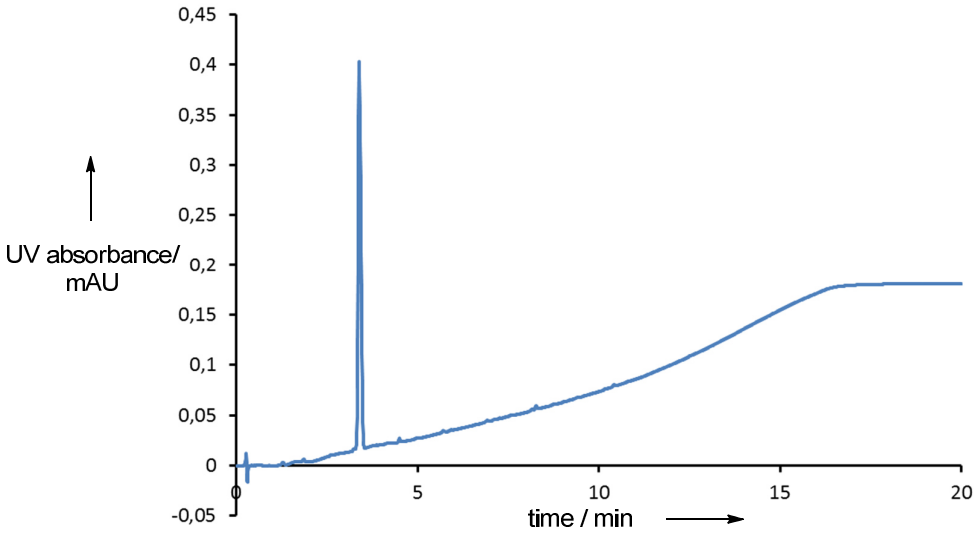

Figure S4. UPLC-UV purity of **TAT** was determined at 220 nm using an Acquity UPLC H-Class operated with Empower 3 software (all Waters Corporation, US) on a C18-column (Acquity UPLC BEH C18 1.7 µm, 2.1 x 50 mm) at constant flow of 0.6 mL/min of 2 % to 100 % acetonitrile in water (with 0.1 % TFA) over 15 min.

3 Protein Biosynthesis

3.1 Strains and Plasmids

The plasmid pET30b_GFPhs1-RM encoding a mutated variant of GFP containing only the N-terminal methionine (Met) (GFPhs1-RM,[1] 245 amino acids, 27.6 kDa) was kindly provided by Soundrarajan Nagasundarapandian from the group of Prof. Sun Gu Lee (Pusan University, South Korea). A Tobacco Etch Virus (TEV) protease recognition site was introduced for removal of the C-terminal His-tag. Glutamine at the N-terminus ensures that the N-terminal Met or homoprogargylglycine (HPG), respectively, is not cleaved.
For expression of GFPhs1-RM_TEV, the Met auxotrophic E. coli strain B834 (DE3) (B→B834[2]→ B834 (DE3)[3] was used.

3.2 Protein Biosynthesis and Purification

Protein biosynthesis was performed using Met auxotrophic *E. coli* strain B834 (DE3).[3] Cells were transformed with pET30b_GFPhs1-RM_TEV. An overnight culture in LB media was used to inoculate the new minimal media expression culture (1:1000).[4] The expression culture containing 45 µM Met as natural substrate was grown at 30°C overnight until depletion of Met and an optical density at 600 nm between 0.6 and 0.7. Defined concentration of the canonical amino acid allows the production of cell mass up to an OD_{600} value of 0.6-0.8. The next day, the Met analogue homopropargylglycine (HPG, Chiralix B. V., Netherlands) was added to a final concentration of 50 mg/ml, and target gene expression was induced by addition of 0.5 mM isopropyl ß-D-1-thiogalactopyranoside. For protein production cells were incubated at 28 °C for four hours with vigorous shaking at 160 RPM. After cell harvest, cells were lysed with sonication and the lysate cleared by high-speed centrifugation (18,000 g, 4 °C, 30 minutes). Soluble target protein was purified from the supernatant using a Ni-NTA column (GE Healthcare, UK) equilibrated with sodium dihydrogenphosphate buffer (50 mM, pH 8) containing 300 mM NaCl, 20 mM imidazole and 5 % glycerol (buffer NA). Unspecifically bound proteins were washed out with 30 mM imidazole and the desired protein was eluted with 500 mM imidazole. Afterwards, the buffer was exchanged via dialysis to TEV reaction buffer (50 mM NaH_2PO_4, 100 mM NaCl, 0.5 mM EDTA, 1mM DTT, pH 8). The C-terminal His-tag was cleaved using TEV protease which was added to the protein and incubated at room temperature overnight. Next, the protein was dialyzed into buffer NA again and His-tagged TEV protease and not-cleaved protein were separated from cleaved protein via a Ni-NTA column. The flow through containing the cleaved protein was collected and dialyzed against storage buffer (50 mM NaH_2PO_4, 100 mM NaCl, 5 % glycerol, pH 8). Protein purity was analyzed by SDS-PAGE and Coomassie staining, whereby protein concentration was determined by measuring the absorption at 280 nm. Incorporation of HPG in GFPhs1-RM was confirmed via ESI-MS (Exactive ESI-Orbitrap-MS, Thermo Fisher Scientific, US). The purified proteins were stored at -80 °C in aliquots until usage.

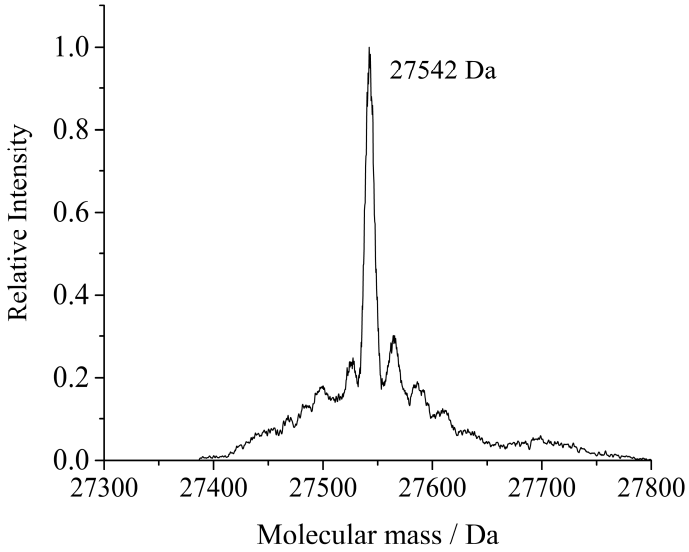

Figure S5. ESI-MS analysis of GFPhs1-RM_TEV with HPG incorporated at the N-terminus. Calculated mass: 27,543 Da, Measured mass: 27,542 Da.

4 Protein-Peptide Conjugation

4.1 Optimized Procedure

Mutant GFP was conjugated with cyclic or linear TAT peptides using CuAAC. Optimized reaction conditions include shaking with 1,000 turns per minute at 15 °C for 20 h in Ca/Mg free Dulbecco's PBS at final concentrations of protein 20 µM, azidopeptide 500 µM, $CuSO_4$ 200 µM, THPTA ligand 1,000 µM and aminoguanidine hydrochloride and sodium ascorbate 10 mM (added stepwise at the start of the reaction and after two hours). For screening of conditions and different azidopeptides, the batch size was 250 µL, conjugation for cell experiments was done at batch size 500 µL. Then, the reaction was quenched with 50 µL of 5 mM EDTA. Copper was removed via dialysis against 2.5 mM EDTA in Ca/Mg free Dulbecco's PBS (three times 400 µL), then EDTA was removed via dialysis against HEPES buffer (three times 400 µL). This was done using centrifugal filters (Amicon Ultra 0.5 mL 10K MWCO regenerated cellulose, Merck Millipore, Merck KGaA, Germany). Full conversion and formation of product was verified using an AB SCIEX TOF/TOF 5800 (Applied Biosystems, Life Technologies, US). For this, 2 µL of the concentrated product were precipitated in 8 µL of acetone. The precipitate was then dissolved in 2 µL mQ water, 2 µL of each DHAP matrix and 2.0 % TFA were added and spotted on the target.

Table S1. Optimized reaction setup with final concentrations and equivalents used.

Reagents added in this order (stock concentration)	Volume / µL testreaction	production	Conc. / µM	Eq.
HPG-GFP (50µM)	100	200	20	1
PBS 1x without Ca,Mg	90	180	-	-
Azido-peptide (50 mM)	2.5	5	500	25
Premixed $CuSO_4$ (20 mM) : THPTA (50 mM) = 1:2	7.5	15	200/1,000	10/50
Aminoguanidine HCl (100 mM)	25	50	10	500
Sodium Ascorbate (100 mM)	15+10	25+25	10	500

4.2 Initial efforts on getting access to pure CPP-GFP conjugates

Initially, we aimed at conjugating a cyclic peptide containing a linker of five amino acids and introduced an azido benzoic acid as reaction handle (**cTAT A**). CuAAC of **cTAT A** and GFP at optimized conditions (testreaction, 15 °C, 20 h, Table S1) lead to 50 percent of conversion (Figure S6). Addition of more copper led to degradation.
Alternatively, we installed azido butanoic acid instead (**cTAT B**) which lead to essentially similar results (Figure S7).

For protein mixtures, plenty of purification methods are available. We rationalized that the charge is the major difference between starting material GFP (pI = 6.3) and conjugation product CPP-GFP (pI = 8.8) which is why we put effort into cation and anion exchange chromatography. Albeit trying different conditions of pH and ionic strength we could only recover traces of protein from the column. Also, we found it impossible to achieve separation with size exclusion chromatography and reversed phase chromatography.

Accordingly, we aimed at a CPP with a thin and flexible linker, which is why we designed the cyclic CPP with a PEG linker (**cTAT**) as reported in this paper. CuAAC with **cTAT** lead to a conversion of 90 to 100 percent (Figure S8 and S10).

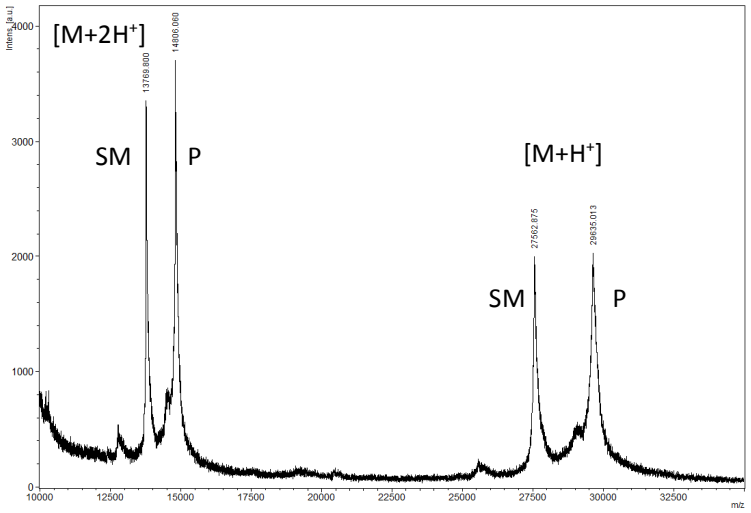

Figure S6. MALDI of testreaction of HPG-GFP and **cTAT A** at conditions given in table S1.

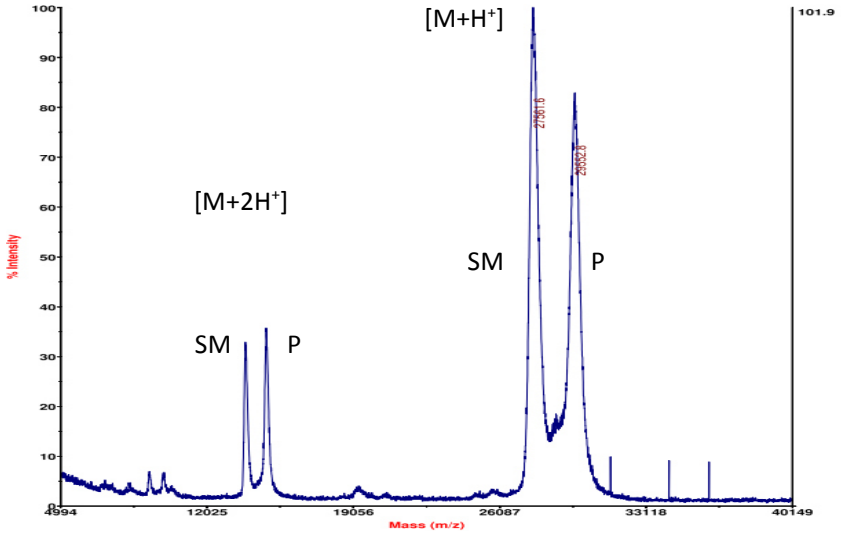

Figure S7. MALDI of testreaction of HPG-GFP and **cTAT B** at conditions given in table S1.

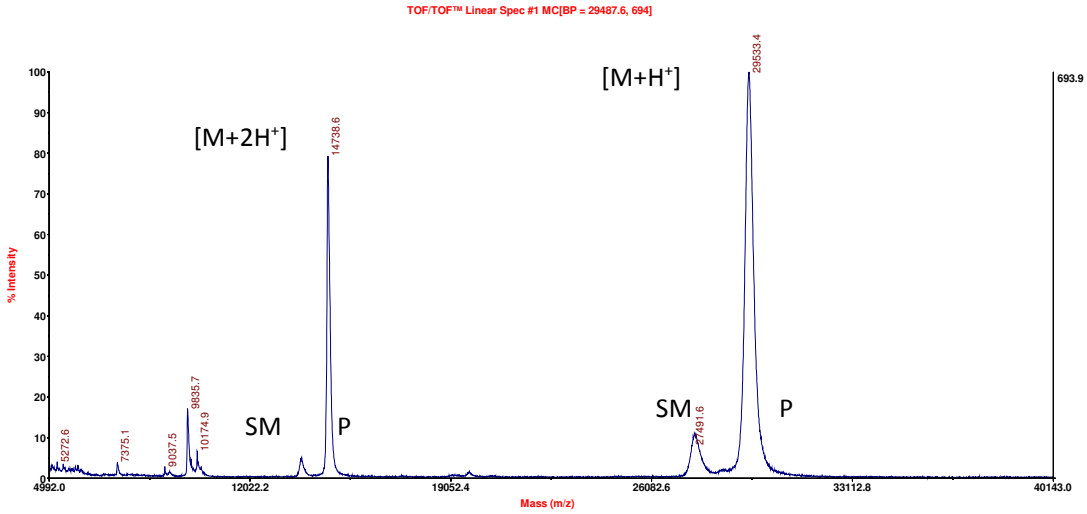

Figure S8. MALDI of testreaction of HPG-GFP and **cTAT** at conditions given in table S1.

4.3 Representative MALDI Spectra of GFP, cTAT-GFP and TAT-GFP

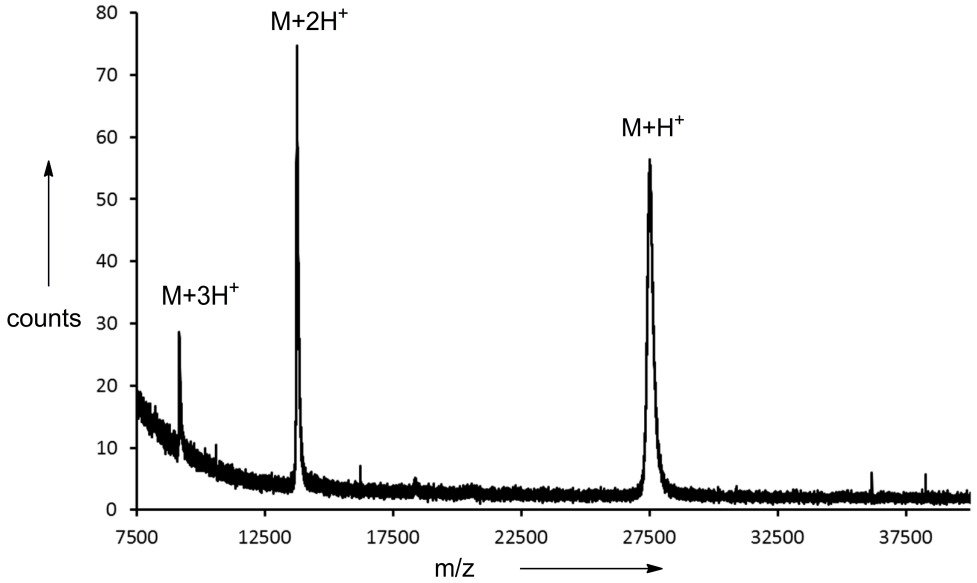

Figure S9. MALDI of **GFP**, expected: 27,543 Da ($M+H^+$), 13,772 ($M+2H^+$), 9,182 ($M+3H^+$), found 27,487 ($M+H^+$), 13,766 ($M+2H^+$), 9,175 ($M+3H^+$).

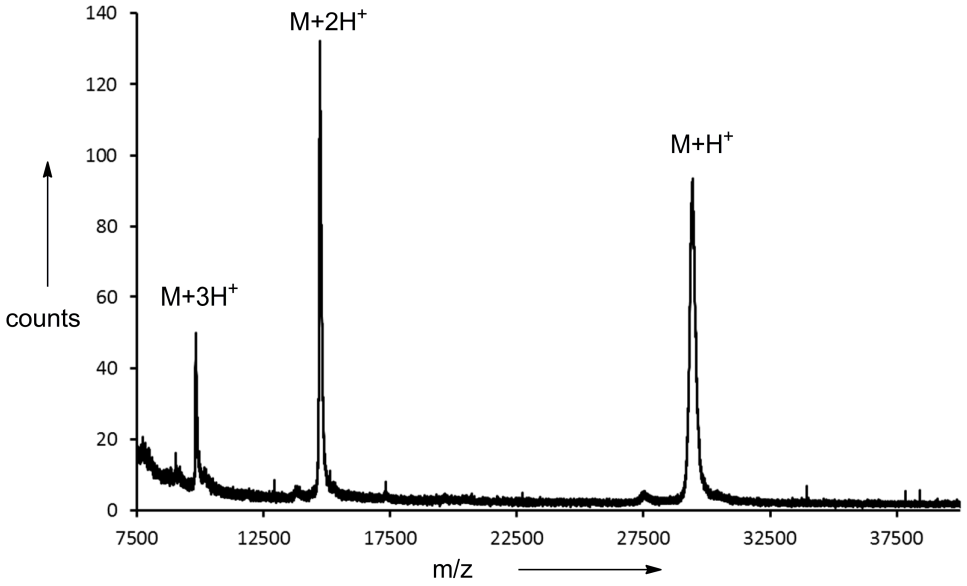

Figure S10. MALDI of **cTAT-GFP**, expected (in Da): 29,451 ($M+H^+$), 14,726 ($M+2H^+$), 9,818 ($M+3H^+$), found (in Da): 29,392 ($M+H^+$), 14,722 ($M+2H^+$), 9,813 ($M+3H^+$).

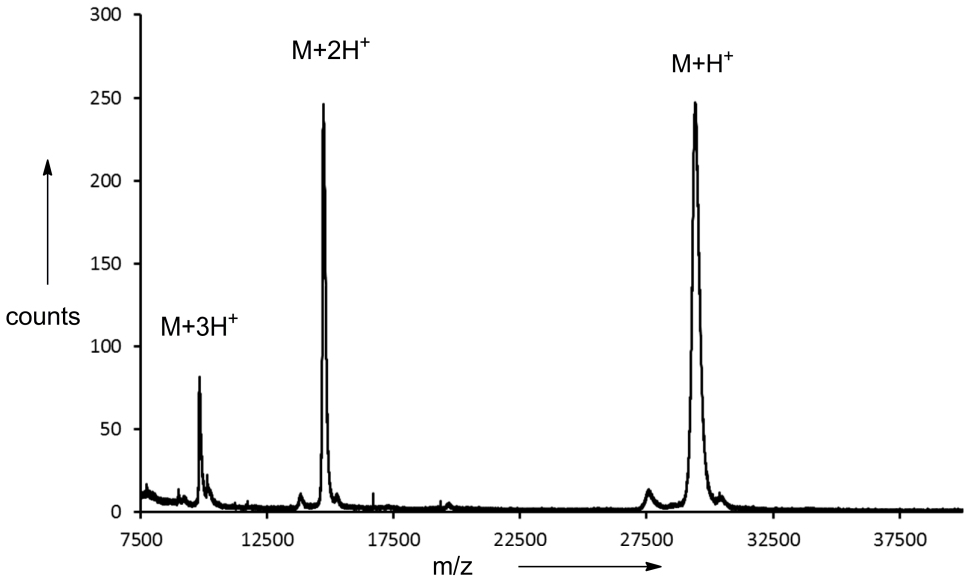

Figure S11. MALDI of **TAT-GFP**, expected (in Da): 29,411 ($M+H^+$), 14,706 ($M+2H^+$), 9,804 ($M+3H^+$), found (in Da): 29,424 ($M+H^+$), 14,716 ($M+2H^+$), 9,822 ($M+3H^+$).

4.4 Photophysical Properties of GFP and cTAT-GFP

Similar aliquots of HPG-GFP were subjected to either optimized reaction conditions (**cTAT-GFP**), reaction conditions without azide (**GFP** mock 1) or without any reagents (**GFP** mock 2), a control stayed frozen (**GFP**). Then all samples were subjected to identical workup procedure consisting of dialysis against EDTA/Dulbecco's PBS and then HEPES buffer as described above.

Then, taking aliquots of each sample and treating them identically, UV absorbance spectra were recorded (Jasco V-630 Spectrometer, Spectra manager, all JASCO Corporation, Japan) as well as the fluorescence emission spectra (Jasco FP-6500 Spectrofluorometer, Spectra manager, all JASCO Corporation, Japan).

Table S2. Reaction setup for comparison of photophysical properties of **GFP** and **cTAT-GFP**.

Reagents added in this order / µL (stock concentration)	**cTAT-GFP**	**GFP** mock 1	**GFP** mock 2	**GFP** (freezer)
HPG-GFP (50µM)	200	200	200	200
PBS 1x without Ca,Mg	180	185	300	0
Azido-peptide (50 mM)	5	0	0	0
Premixed $CuSO_4$ (20 mM) : THPTA (50 mM) = 1:2	15	15	0	0
Aminoguanidine HCl (100 mM)	50	50	0	0
Sodium Ascorbate (100 mM)	25+25	25+25	0	0

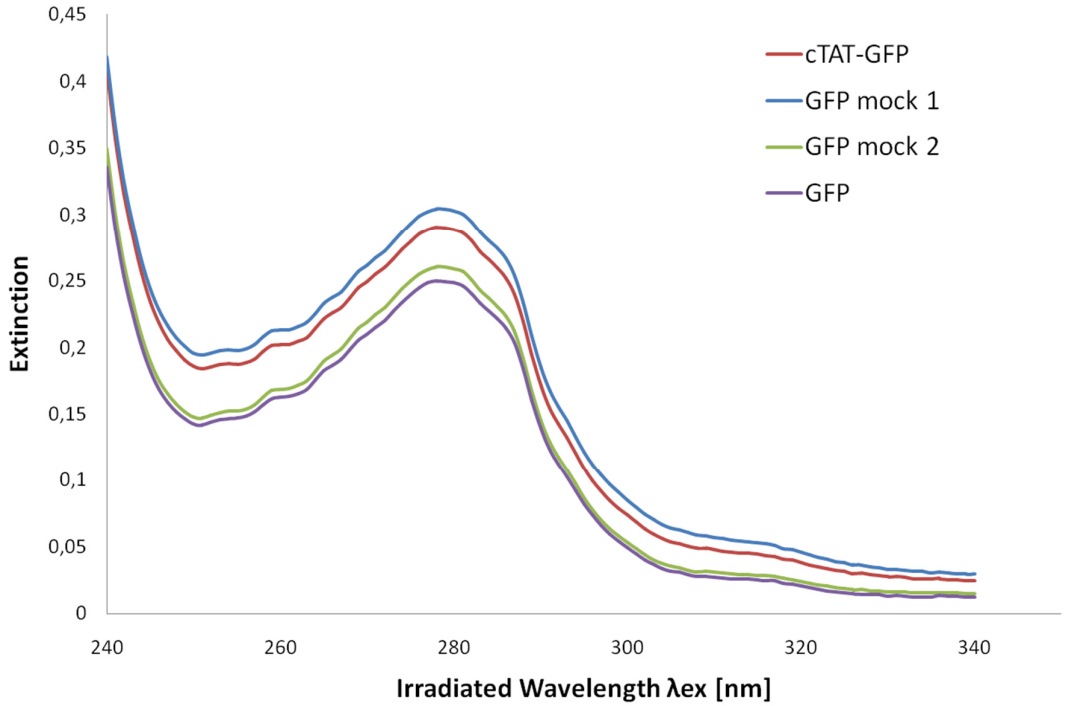

Figure S12. UV absorption spectra with focus on 280 nm to confirm similar protein concentration.

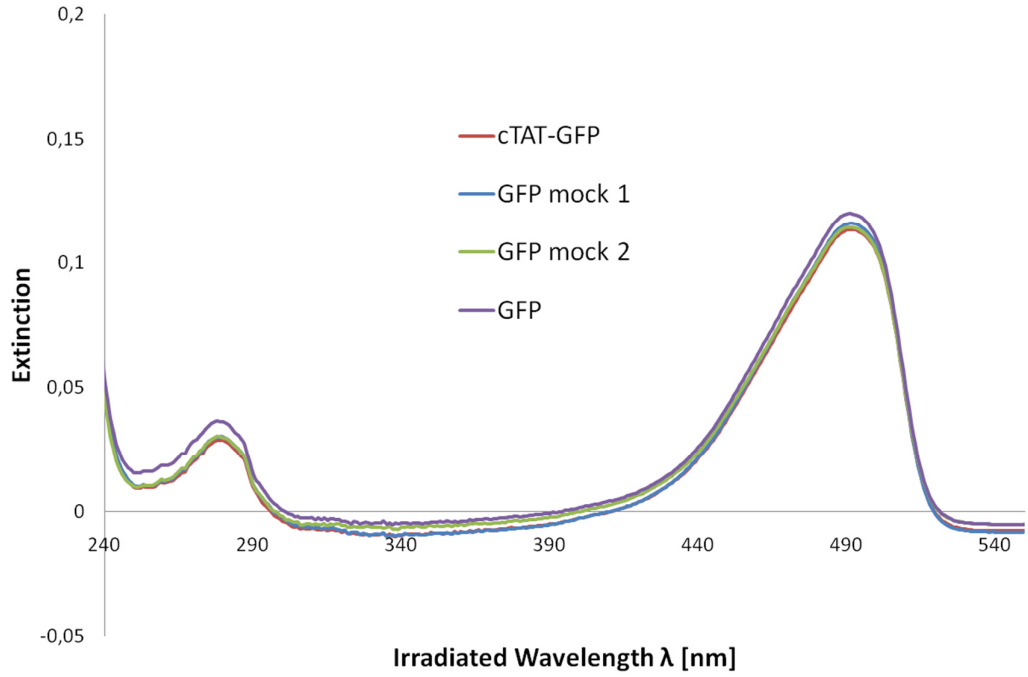

Figure S13. Full UV-Vis absorption spectra to confirm similar absorption maxima at 495 nm.

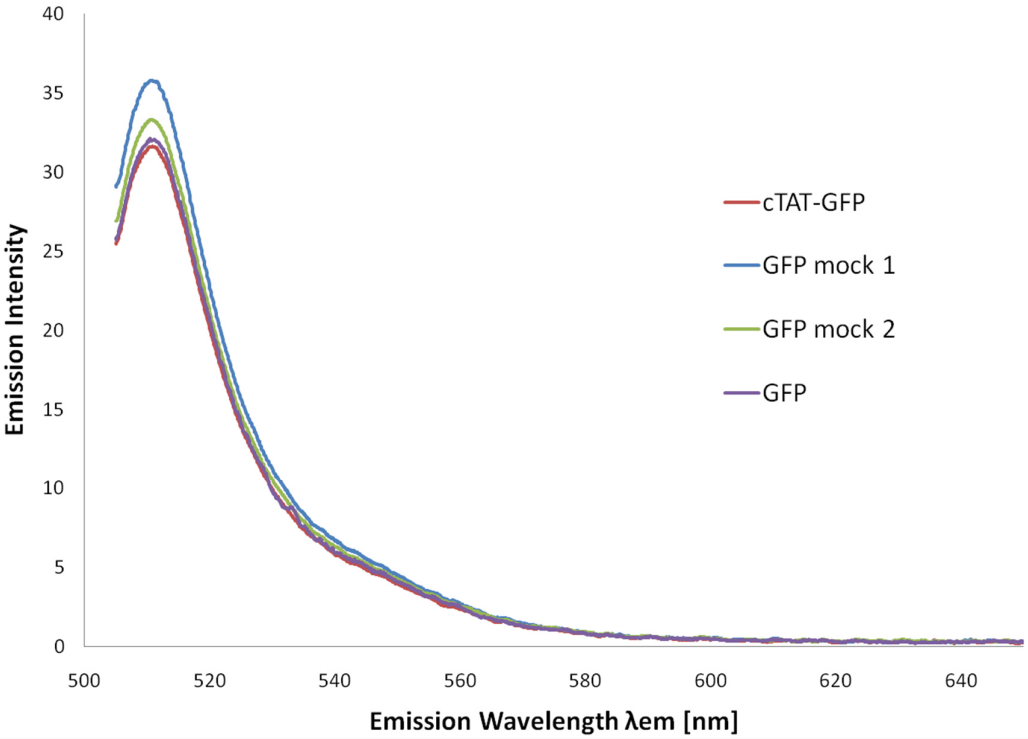

Figure S14. Fluorescence emission spectrum after irradiation at 495 nm confirm similar emission maxima at 509 nm.

5 Cellular Uptake

HeLa (human cervical carcinoma) cells were cultured under standard established conditions as indicated elsewhere.[2c] Cells were seeded at subconfluent concentration in optically proficient 0.17 mm glass bottom multiwell chambers (Evotec, Germany) the day before the live cell microscopy experiments were performed.

5.1 Cellular Uptake by Transduction Versus Endocytosis

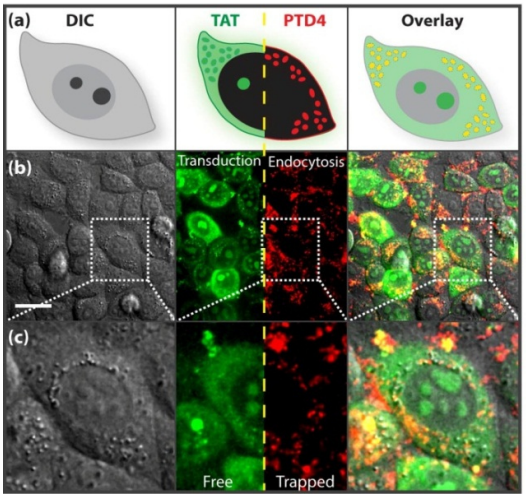

Figure S15. Cellular transduction and endocytic uptake in live cells. **TAT-FITC** and **PTD4-TAMRA** peptides were added to cultured media without serum and cells were incubated at 37°C. Left, differential interference contrast (DIC) images; middle, TAT (green) and PTD4 (red); right, overlay. (a) Representative cartoon, (b) Field captured with several cells, (c) Magnification of a single cell. Scale bar: 15 µm.

5.2 Live Cell Confocal Microscopy of Transduced Cells

Figure S16. Live cell confocal images of the **GFP**, **TAT-TAMRA** and **cTAT-GFP** before and after washing. (a) **GFP** added to the extracellular medium, (b) **TAT-TAMRA** peptide added simultaneously with uncoupled **GFP**, (c) **cTAT-GFP**. Scale bar 15 µM.

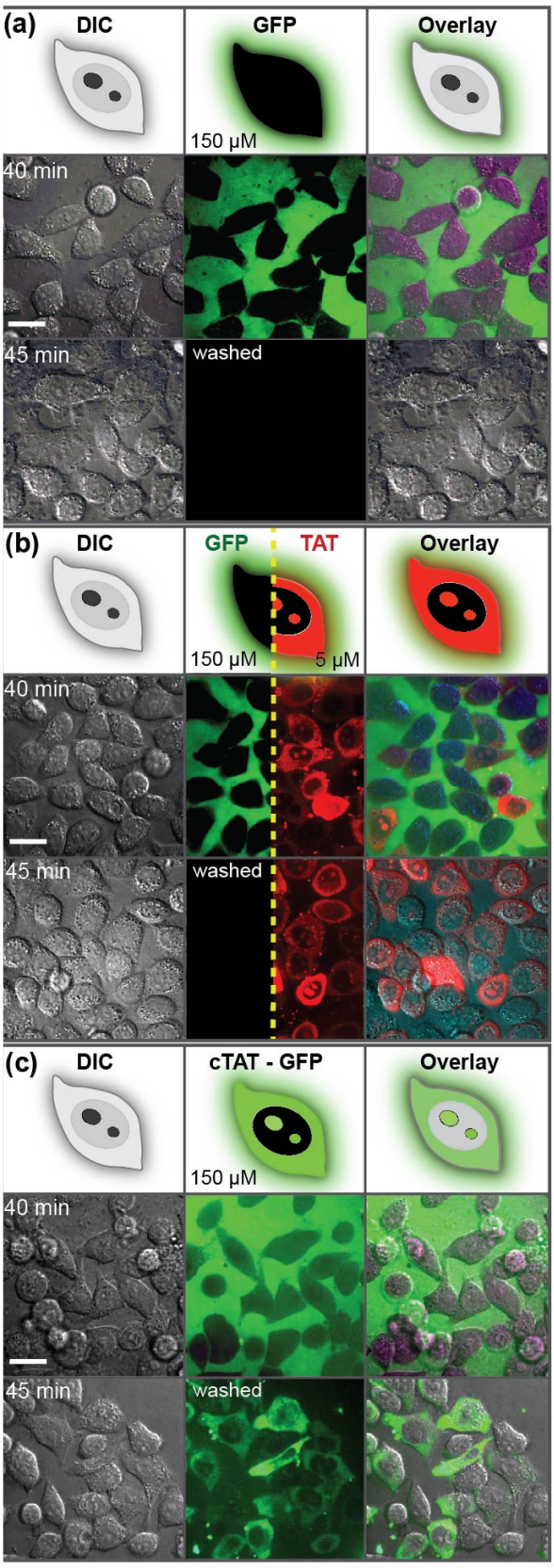

5.3 Fluorescence Recovery After Photobleaching of Internalized GFP

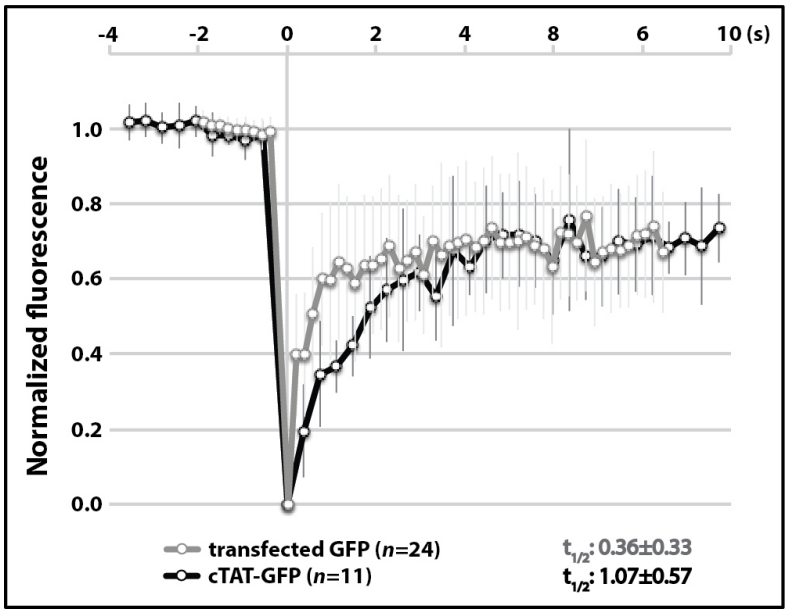

Figure S17. The normalized fluorescence signal is plotted as a function of time (in seconds). Cells transfected with GFP (*n*=24) or transduced by 150 µM **cTAT-GFP** (*n*=11) were photobleached with 488 nm laser at full power for 100 ms in the nucleus or cytoplasm. Transfected GFP was employed as a control for maximal free diffusion ($t_{1/2}$=0.36±0.33 s). Fluorescence recovery of **cTAT-GFP** transduced cells ($t_{1/2}$=1.07±0.57 s) was comparable to that of transfected GFP, indicating that the transduced molecules are freely diffusing inside the cell. These observations are in agreement with our previous findings.[5] The slight different kinetics we observed can be attributed to the positively charged residues of the cTAT peptide influencing the interactions between the transduced protein and the crowded intracellular environment. Fluorescence recovery was measured at a speed of one frame per 192 or 374 ms for transfected GFP or **cTAT-GFP** transduced cells, respectively.

5.4 Cellular Uptake Does Not Require Macropinocytosis or Metabolic Energy

Currently, the two main proposed mechanisms of uptake for arginine-rich peptides, such as the TAT peptide, are macropinocytosis and either direct translocation across the plasma membrane at lower concentrations or transduction at higher concentrations.[6] Macropinocytosis requires metabolic energy while transduction is energy independent. In the present work we initially found that **cTAT-GFP** is able to get into cells in a HEPES buffer depleted from nutrients. This suggests that macropinocytosis or other energy dependent pathways might not be mandatory in the cellular uptake of **cTAT-GFP**, following in this way a similar mode of uptake as arginine-rich peptides.[6c] To directly investigate if macropinocytosis is involved in the mode of cellular entry of the **cTAT-GFP** complex we tested this uptake in the presence of amiloride, which is a specific macropinocytosis inhibitor. The formation of macropinosomes appears to be distinctively inhibited by amiloride and its analogues, and this property has been extensively used as an identifying feature of micropinocytosis.[7] As shown in Fig. S18 (a), in the presence of amiloride at 1mM we found uptake of **cTAT-GFP** in 76 % of the cells.

To strictly assess that the pathway of cell entry does not require metabolic energy, the delivery of **cTAT-GFP** was also carried out at 4 °C. Cells were incubated for 1 hour at 4 °C (or less) in a HEPES buffer lacking nutrients and glucose. Then the cells were placed on ice and the protein complex in solution (also kept in ice previously for 1 hour in a HEPES buffer) was added to the cells and incubated for an extra 40 min at 4 °C. The cells were washed three times with PBS and imaged immediately at the confocal microscope. The same protocol was simultaneously done for the TAT peptide (**TAT-TAMRA**) to compare the **cTAT-GFP** uptake side by side with the uncoupled TAT peptide. We detected uptake in all cases Fig S18 (b-d). In all cases **cTAT-GFP** and **TAT-TAMRA** were found in most cells freely distributed in the cytosol and labeling distinctively the nucleolus. The only difference was the intracellular intensity that was reduced at the lower concentration of the TAT peptide. This experiment rules out the requirement of any energy dependent cellular uptake pathway, including all endocytotic pathways, since at 4 °C all energy depending pathways are inhibited.
The DIC images show also that the cells remain morphologically healthy and we could see that after raising the temperature to 37 °C the cells continue undergoing cell division.

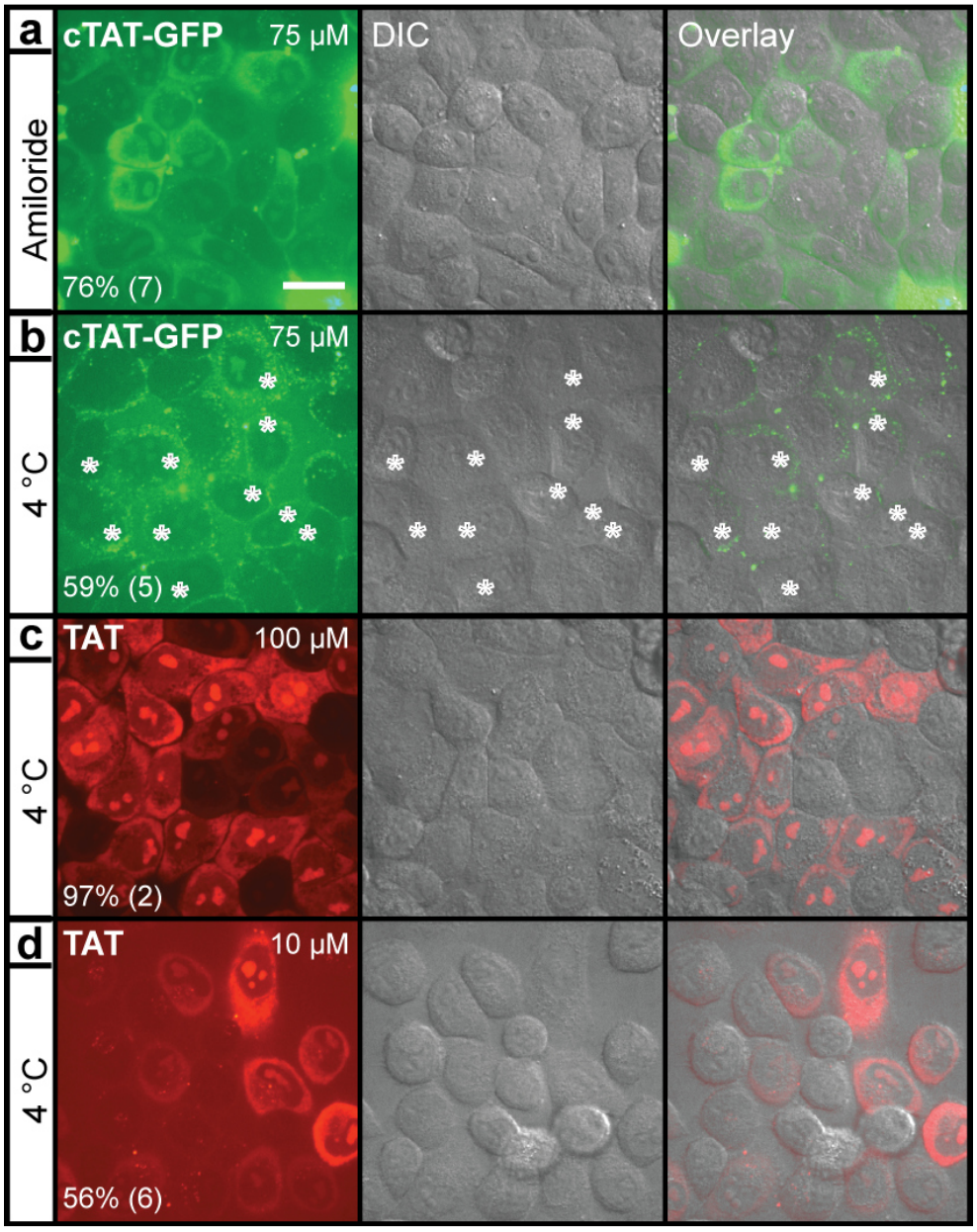

Figure S18. Cellular uptake of **cTAT-GFP** does not require macropinocytosis or any other energy-dependent pathway. (a) Cellular uptake of **cTAT-GFP** (75 µM) in the presence of a macropinocytosis inhibitor (amiloride at 1mM). We found uptake in 76 % of the cells. (b) Cellular uptake of **cTAT-GFP** at 4 °C in a HEPES buffer lacking nutrients and glucose. These conditions completely stop all cellular pathways that require metabolic energy. Under these conditions we still found uptake in 59 % of the cells (cells displaying nucleoli labeling by GFP in this case are explicitly marked with a star sign). (c) Uptake of 100 µM of **TAT-TAMRA** at 4 °C. (d) Uptake of 10 µM of **TAT-TAMRA** at 4 °C. Each experiment was repeated 3 times. The cellular uptake was quantified by counting as positive the cells that displayed clear nucleoli GFP or TAMRA labeling. Standard errors are shown between parentheses. Scale bar 15 µM.

5.5 Quantification of GFP Intracellular Concentration

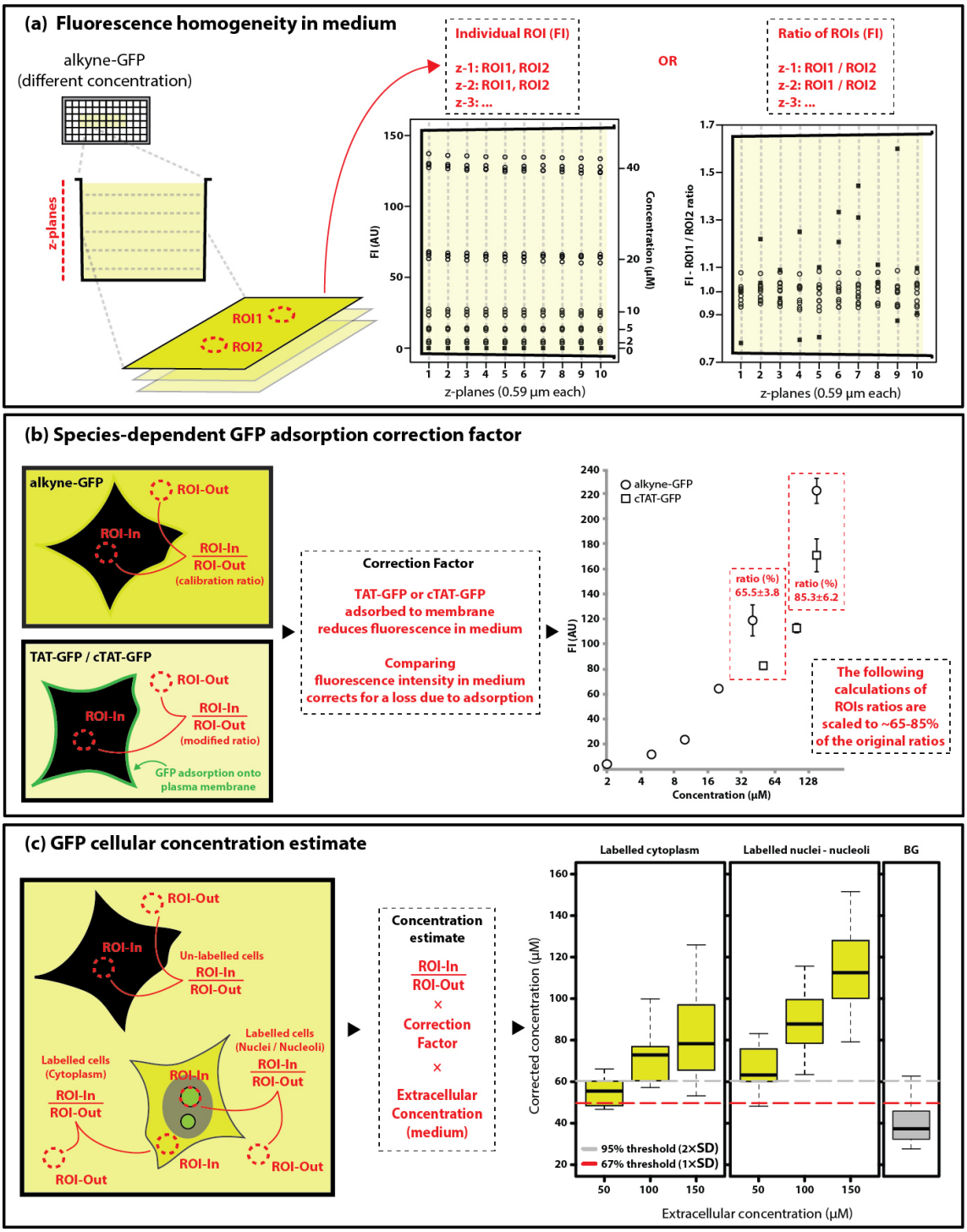

Figure S19. Quantification of intracellular GFP. (a) Alkyne-**GFP** solution was prepared at different concentrations (40, 20, 10, 5, 2 μM) in an optically proficient micro-well dish. Fluorescence intensity (FI) of each micro-well was imaged by confocal microscopy over 10 z-planes (z = 0.59 μm). Two different ROIs per field per z-plane, and at least two fields were imaged. FI of each ROI was plotted as a function of z-planes. Each empty circle represents one ROI. Note how FI is homogenous over ROIs or z-planes, and proportional to **GFP** concentration (left graph). The ratio of two ROIs per field was

plotted as a function of z-planes in the right graph. The ratio is homogenous over z-planes as well as concentrations (overall: 0.99±0.03). Solid squares: negative control of fluorescence (HEPES buffer without alkyne-**GFP**).
(b) FI of ROIs inside or outside the cell contour from alkyne-**GFP** as well as **cTAT-GFP** or **TAT-GFP** was collected over z-planes. Importantly, cells are incubated as described in the methods and the imaging was performed before washing away the incubation solution. While alkyne-**GFP** was inert and its fluorescence remained unchanged in the medium, **cTAT-GFP** or **TAT-GFP** was partly adsorbed onto the plasma membrane. This is mainly due to the CPP moiety conjugated to GFP, which tends to interact with the plasma membrane. Hence, we observed that the FI of the medium is non-linearly reduced by a significant amount in samples treated with **cTAT-GFP** or **TAT-GFP**, compared to those which were treated with alkyne-**GFP**. The graph on the right shows the FI of ROIs from the extracellular space for alkyne-**GFP** (circles) and **cTAT-GFP** (squares) as a function of extracellular concentration. Note how FI of **cTAT-GFP** is lower than that of alkyne-**GFP** at the same concentration. Preliminary observations indicate a FI loss of ~15-35%. Such loss is expressed by the ratio between FI of ROIs in the extracellular space from samples treated with **cTAT-GFP** or **TAT-GFP** or alkyne-**GFP** ($FI_{(c)TAT\text{-}GFP}$ / $FI_{alkyne\text{-}GFP}$), respectively. The loss of fluorescence was taken into account (as a correction factor) to further estimate GFP intracellular concentration.
(c) To estimate GFP intracellular concentration in subcellular compartments (e.g. cytoplasm or nuclei), the ratios of indicated ROIs were calculated. Such ratios were then corrected by the aforementioned correction factor. The corrected ratios were finally multiplied by the original GFP extracellular concentration in the medium. On the right side, the distribution of labelled cells (cytoplasm and nuclei) is shown for 50, 100, 150 μM **cTAT-GFP** (green boxes). Corrected concentration for unlabeled cells is shown in grey and was used to calculate a transduction threshold. The latter are indicated by dashed red and grey lines set at one and two standard deviations above the mean corrected concentration of the unlabeled cells, respectively.

5.6 Movie of Transduced Cells – Motility and Mitosis

Movie 1. cTAT-GFP transduced cells continue moving and undergoing mitosis. First is shown a larger area capturing the motility of a cell followed by mitosis. Both are complex metabolic pathways that require the cell to be viable as well as having an active complex enzymatic network. This is followed by a number of cells undergoing mitosis at different times (indicated in the upper right corner of the DIC images) after being transduced by **cTAT-GFP**.

6 References

[1] S. Nagasundarapandian, L. Merkel, N. Budisa, R. Govindan, N. Ayyadurai, S. Sriram, H. Yun, S. G. Lee, *Chembiochem* **2010**, *11*, 2521-2524.

[2] W. B. Wood, *J. mol. Biol.* **1966**, *16*, 118-133.

[3] a) F. W. Studier, P. Daegelen, R. E. Lenski, S. Maslov, J. F. Kim, *J. mol. Biol.* **2009**, *394*, 653-680; b)F. W. Studier, B. A. Moffatt, *J. mol. Biol.* **1986**, *189*, 113-130.

[4] C. Minks, S. Alefelder, L. Moroder, R. Huber, N. Budisa, *Tetrahedron* **2000**, *56*, 9431-9442.

[5] G. Tunnemann, R. M. Martin, S. Haupt, C. Patsch, F. Edenhofer, M. C. Cardoso, *Faseb J.* **2006**, *20*, 1775-1784.

[6] a) R. Brock, *Bioconjug Chem* **2014**, *25*, 863-868; b) I. M. Kaplan, J. S. Wadia, S. F. Dowdy, *J. Contr. Release* **2005**, *107*, 571-572; c) G. Ter-Avetisyan, G. Tunnemann, D. Nowak, M. Nitschke, A. Herrmann, M. Drab, M. C. Cardoso, *J. Biol. Chem.* **2009**, *284*, 3370-3378; d) H. D. Herce, A. E. Garcia, J. Litt, R. S. Kane, P. Martin, N. Enrique, A. Rebolledo, V. Milesi, *Biophys. J.* **2009**, *97*, 1917-1925; e) H. D. Herce, A. E. Garcia, *J. biol. Phys.* **2007**, *33*, 345-356.

[7] a) M. Koivusalo, C. Welch, H. Hayashi, C. C. Scott, M. Kim, T. Alexander, N. Touret, K. M. Hahn, S. Grinstein, *J. Cell Biol.* **2010**, *189*; b) M. A. West, M. S. Bretscher, C. Watts, *J. Cell Biol.* **1989**, *109*, 2731-2739; c) A. Veithen, P. Cupers, P. Baudhuin, P. J. Courtoy, *J. Cell Sci.* **1996**, *109*, 2005-2012; d) O. Meier, K. Boucke, S. V. Hammer, S. Keller, R. P. Stidwill, S. Hemmi, U. F. Greber, *J. Cell Biol.* **2002**, *158*, 1119-1131.

7 Appendix

cTAT: HRMS. Measured on a LCT Premier Micromass Technologies system (a) Table of calculated m/z that correspond to found masses, (b) full ESI-MS spectrum and (c) zoom on the five times protonated mass.

(a)

protonation	2x	3x	4x	5x
M		637.0572	478.0449	382.6375
M + 1 TFA		675.0539	506.5424	405.4355
M + 2 TFA		713.0506	535.0399	
M + 3 TFA	1126.0670	751.0472		
M + 4 TFA	1183.0620			
M + 5 TFA	1240.0570			

(b)

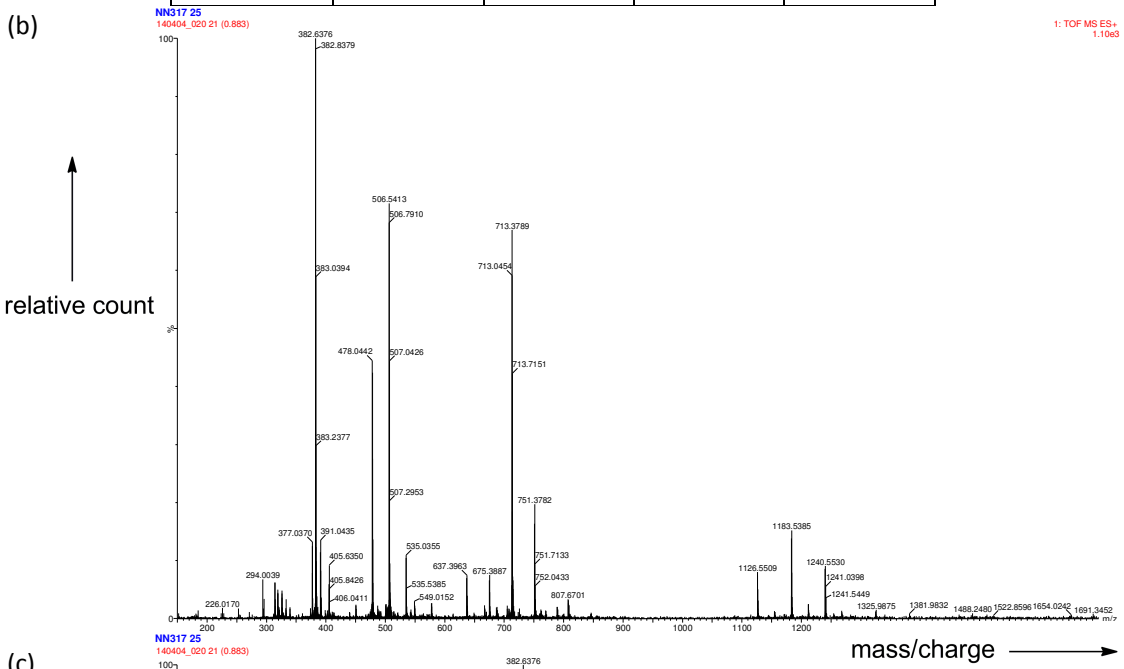

(c)

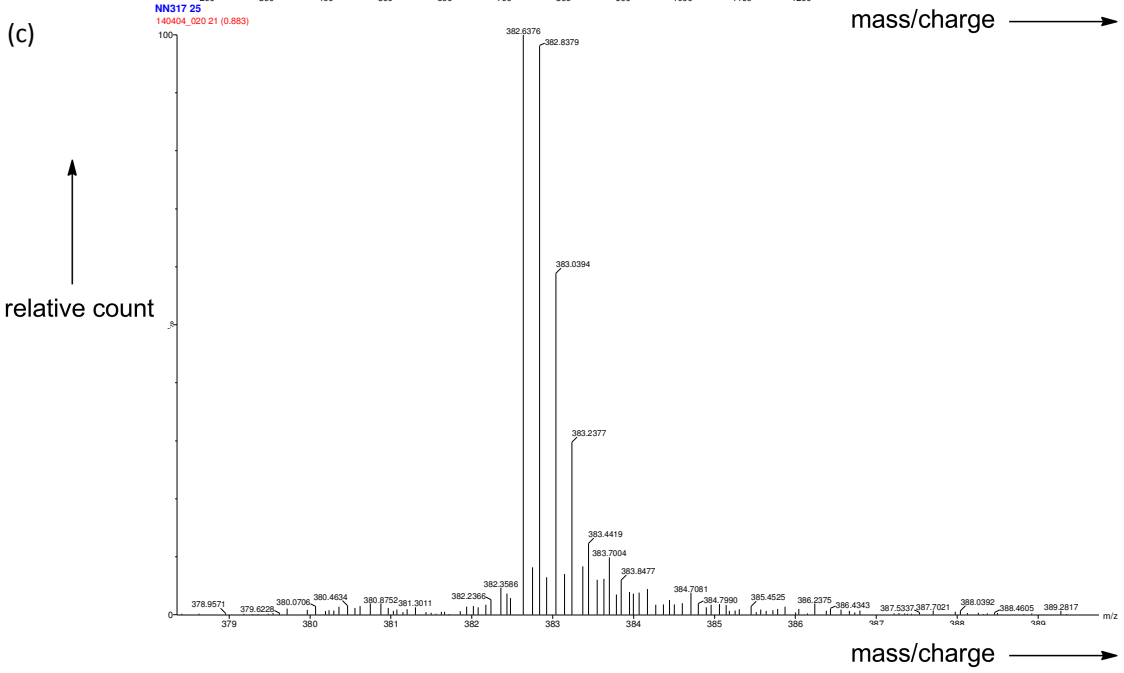

cTAT A: HRMS. Measured on a Agilent 6210 ToF LC-MS system (a) Table of calculated m/z that correspond to found masses, (b) full ESI-MS spectrum and (c) zoom on the five times protonated mass.

(a)

protonation	2x	3x	4x	5x
M	1033.6005	689.4030	517.3042	414.0449
M + 1 TFA	1090.5955	727.3996		
M + 2 TFA	1147.5905			

(b)

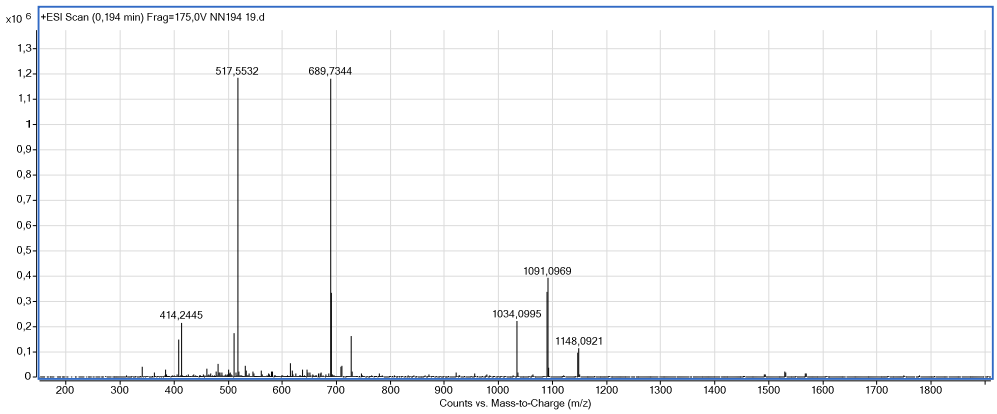

(c)

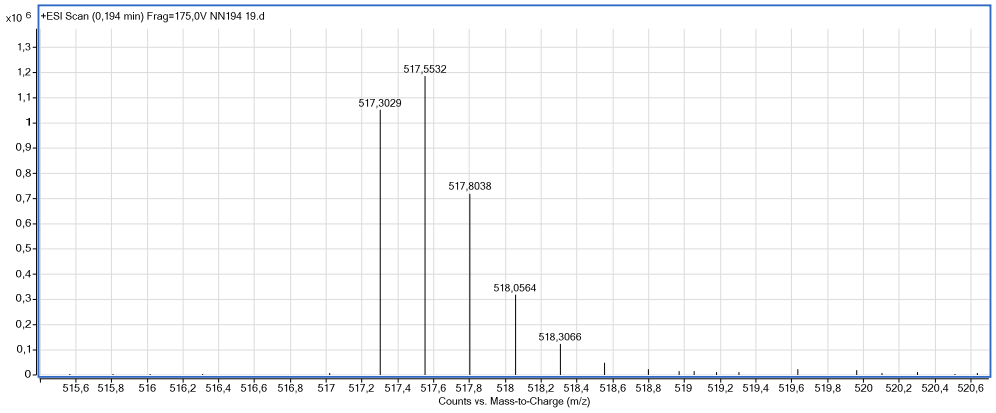

cTAT B: HRMS. Measured on a Agilent 6210 ToF LC-MS system (a) Table of calculated m/z that correspond to found masses, (b) full ESI-MS spectrum and (c) zoom on the five times protonated mass.

(a)

protonation	2x	3x	4x
M	1026.6083	678.0748	508.8081
M + 1 TFA	1073.6033	716.0715	
M + 2 TFA	1130.5983		

(b)

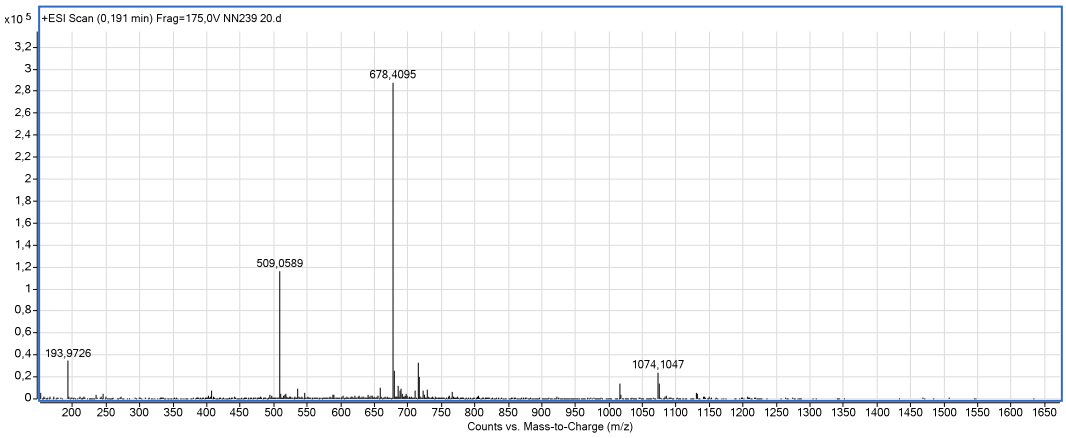

(c)

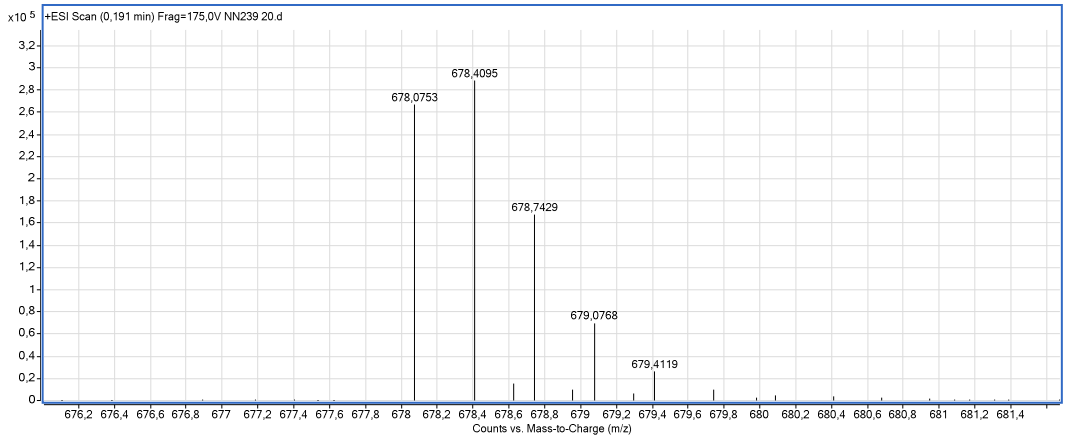

TAT: HRMS. Measured on a LCT Premier Micromass Technologies system (a) Table of calculated m/z that were correspond to found masses, (b) full ESI-MS spectrum and (c) zoom on the five times protonated mass.

(a)

protonation	2x	3x	4x	5x	6x
M		623.7129	468.0366	374.6309	312.3603
M+1 TFA		661.7096	496.5341		
M+2 TFA		699.7062	525.0316		
M+3 TFA	1106.0504	737.7029			
M+4 TFA	1163.0454				
M+5 TFA	1220.0404				

(b)

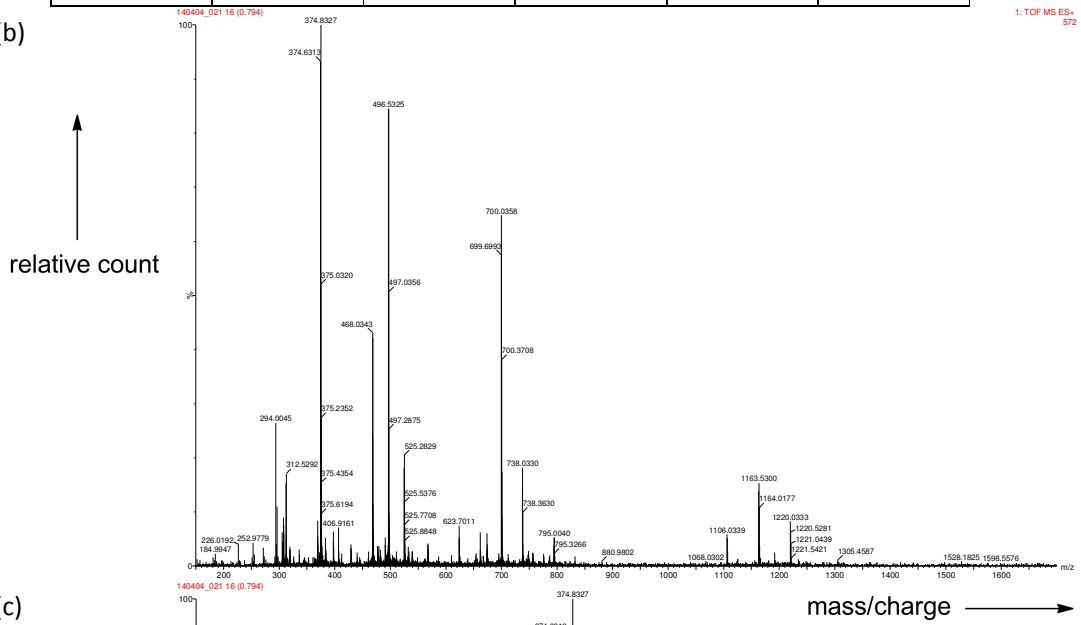

(c)